Modelling the adsorption and controlled release of drugs from the pure and amino surface-functionalized mesoporous silica hosts

A. Martín, V. Morales, J. Ortiz-Bustos, M. Pérez-Garnes, F. Bautista, R. A. García-Muñoz and R. Sanz*

Chemical Engineering Group, Universidad Rey Juan Carlos, C/ Tulipán s/n, 28933 Móstoles, Madrid, Spain

* corresponding author: raul.sanz@urjc.es

Abstract

Several mesoporous silica materials with different structures were investigated as matrices for controlled drug delivery. The aim of this study is correlating the textural and surface chemical properties of these materials with the adsorption and delivery of the drug model methylprednisolone sodium succinate. The materials were synthetized according to different protocols, and employing both cationic and non-ionic surfactants. Additionally, the functionalization of the materials' surface with 1-[3-(trimethoxysilyl)propyl]diethylenetriamine (DT) was accomplished to study the synergistic effect of the incorporation of amine groups and textural properties on the loading and delivery of drug. The thermodynamics and dynamic adsorption behavior of these materials were determined and fitted to several isotherms models to provide information about the drug adsorption processes. The maximum adsorption capacities of the raw silica supports were correlated with the pore size and the results indicated that the drug adsorption ability improved as the material pore size increases. Moreover, it is observed that the drug adsorption on materials with mesoporous size higher than 10 nm are very close to the theoretical saturation capacity. Regarding amino-modified materials, isotherms models confirmed that the factor governing the adsorption process were mainly the electrostatic interactions, hydrogen bonding and/or hydrophobic-hydrophilic interactions between the drug moieties and amino-functionalized silica surfaces, and in a lesser degree the textural properties of the silica support. Furthermore, the kinetics of the methylprednisolone sodium succinate release from these materials functionalized with amino groups were also

modelled to finally obtain a correlation between the adsorption and release drug cargo from the host pure and surface-functionalized silica materials. Finally, it was confirmed that cell viability was largely unaffected by amino-functionalized mesoporous SBA-15 materials after 72 h of incubation time.

Keywords: ordered mesoporous materials, methylprednisolone, adsorption and release drug processes, drug controlled release

1. Introduction

In the last years, ordered mesoporous silica materials have emerged as novel platforms for applications such as biomedical to support enzyme´s immobilization, electrochemical and optical sensors, heterogeneous catalysis, and biomolecule separation [1-5]. More recently, since 2000, the application of mesoporous silica materials as drug carriers to control the drug delivery has experienced an outstanding growing. These mesostructured silica materials have been identified as potentially effective drug delivery systems (DDS) due to their remarkable control and sustained release of different pharmacologically active substances as a consequence of their high surface area, pore volume and porosity, which involves to tailor materials with different morphologies (spheres, tubes, cylinders, ….) and with linear, tortuosity, roughness, smooth, or interconnected porosity [6-13]. The key point in drug delivery is that the DDS need to be biocompatible, which is essential for the safety and drug efficiency, and also they have to exhibit a high capacity for loading and preventing the leakage of the drug cargo before reaching the target organ. In addition, drug molecules must release in a controlled/sustained way and with a proper rate to achieve therapeutic activity with minimal side effects [14-18]. The dosage and the delivery rate of a particular drug can be controlled with great efficiency by modifying one or more of the following parameters: the structure and composition of the matrix [19, 20], the pore size [21, 22], pore entrance modification [23, 24], and the chemical interaction with the host [25]. Mesoporous silica structures are also characterized by their proved biocompatibility [26-

28] and because they can be easily modified with different functionalities, which allow accurate control of surface chemistry to modulate the chemical activity, hydrophobicity or hydrophilicity, drug loading, sustained release and site specific targeting [29-35].

Typically, two methods are used for the introduction of organic groups onto the silica surface: co-condensation [36, 37] and post-synthesis grafting [38, 39]. The accessibility to the loaded organic moieties is higher in the case of grafting method since the reaction of organosilane species with the silanol groups takes place at the silica surface. This fact enables stronger interactions between the drug molecules and organosilane moieties anchored onto the mesoporous silica materials [24, 40-41].

Among the great bunch of organic functionalities that can be incorporated into the silica surface, those containing amino groups are widely reported in literature as a consequence of the electrostatic interactions that can exert with the drug guests, and therefore affecting the drug adsorption capacity of the silica supports [39, 42-44]. In this work, we have functionalized by grafting different silica supports using an organosilane containing three amino groups on its structure, 1-[3-(trimethoxysilyl)propyl]diethylenetriamine (DT). The selection of this compound was based in a previous works in which was determined the high affinity between this specific organosilane and the model drug used in this work [40].

The corticoid methylprednisolone sodium succinate (Scheme S1) has been chosen as drug delivery model. This molecule possesses hydrophilic features, which permits a high solubility in water and it possesses immunosuppressive and anti-inflammatory properties. Its administration relieves inflammation and it is prescribed for the treatment of arthritis; skin and intestinal disorders; thyroid; severe allergies; and asthma. A particular application is focused to the treatment of rhinosinusitis, a disease of nasal mucosa, which is accompanied by acute or chronic inflammation. Oral administration has been the conventional treatment in chronic rhinosinusitis, but in the field of oral medicine, some ingested drugs were used to cure nasal

diseases, which are normally administered in pill or tablet form. Unfortunately, they may be adsorbed, digested or breakage in the low pH conditions of the stomach. Therefore, in order to carry out the cure efficacy in respiratory system, it is needed an alternative method to design a drug-delivery system which ensures that an effective drug concentration reaches the specific site to develop the physiological action.

The aim of this work is to investigate the influence of the structural characteristics (pore size, structure and morphology type) of several raw mesoporous silica materials with different structures, as well as their amino-modified counterparts to understand their effect on the adsorption and release of the drug model chosen, methylprednisolone sodium succinate, to permit a comparison with other results of similar mesoporous silica materials reported in the literature. The textural properties of raw mesoporous silica materials are pivotal to determine their drug adsorption and delivery capacities. Otherwise, the amino-modified counterpart materials based their effectiveness as drug delivery systems on the electrostatic interactions and hydrogen bonding that the amino surface-functionalized mesoporous silica and the drug guest exert mutually. To establish the ability that these mesoporous silica materials present to adsorb the drug cargo, the thermodynamics and dynamic adsorption behavior were determined and fitted to several isotherms models. Moreover, the kinetics of the drug model release from these materials were also modelled to finally obtain a comprehensive insight of the adsorption and release pharmaceutical methylprednisolone sodium succinate from the host silica materials. This study could be handle as a model to provide a guidance to select and design novel mesoporous siliceous adsorbents for other drugs.

2. Experimental

All materials were purchased from Sigma Aldrich and used as received, except hydrochloric acid and anhydrous toluene that were purchased from Scharlab.

2.1 Synthesis of pure silica supports and amino-modified mesoporous materials

The synthesis of the used silica mesoporous materials (SBA-3, MCM-41, MH, SBA-16, LP-FDU-12, SBA-15, PHTS, LP-SBA-15, MCF and ULP-SBA-15) was accomplished using previously described methods, which are summarized in supplementary information.

Prior to the functionalization process by post-synthesis grafting, and in order to increase the number of surface silanol groups, a rehydroxylation process was carried out by refluxing the calcined silica supports in hydrochloric acid (18.5% w/w) for 12h. Subsequently, the rehydroxylated materials were carefully vacuum-dried, sealed under vacuum, and subsequently subjected to argon atmosphere. It has been reported that this method leads to an increase in the surface silanol concentration from 2 to 5 $\mu mol \cdot m^{-2}$ for mesoporous SBA-15 materials without observing loss of ordering for the treated samples [46].

Post-synthesis grafting consists on the reaction between the rehydroxylated supports (1 g) and the corresponding amount of 1-[3-(trimethoxysilyl)propyl]diethylenetriamine (DT) (10 and 30 % molar ratios). The reactions were carried out under nitrogen atmosphere with anhydrous toluene and stirring at 60 ℃ for 24h. The resulting solids were filtered and washed with toluene and acetone in order to remove the excess of non-reacted organosilane, dried under vacuum at room temperature overnight, and stored in a drybox [47].

Functionalized mesoporous silica materials were denoted as SBA-3-10DT, MCM-41-10DT, MH-10DT, SBA-16-10DT, LP-FDU-12-10DT, SBA-15-10DT, PHTS-10DT, LP-SBA-15-10DT, MCF-10DT, ULP-SBA-15-10DT, SBA-15-30DT, LP-SBA-15-30DT and MCF-30DT in the forthcoming text.

2.2 Corticoid loading

Methylprednisolone sodium succinate was loaded into the supports by the solvent adsorption methodology from a highly-concentrated solution of the drug. For the equilibrium isotherms, the pure silica and functionalized materials (0.1 g) were added to a solution of methylprednisolone sodium succinate in growing concentrations of 0.5, 2.5, 5, 10, 15, 20, 25, 30

and 35 mg/mL in water (10 mL). These suspensions were stirring at 260 rpm during 24h at 25 ℃ while the evaporation of water was prevented in a glass tube. The suspensions were centrifugated at 3500 rpm during 10 minutes after which the supernatant was separated and the impregnated solids were dried overnight at 70 ℃ in a vacuum oven.

The determination of the methylprednisolone sodium succinate loading in the material was measured spectrophotometrically at a wavelength of 247 nm in a UV-Spectrometer (JASCO V-630) by the difference between the initial concentration and the concentration of drug in the supernatant.

2.3 Drug release assay

Sterilized dialysis bags with dialyzer-weight cut-off 10,000 Da were used to carry out the drug release experiments, although they were pretreated prior to use as follows. These dialysis bags were fully immersed into 50 % aqueous solution of ethanol at 40 ℃ during 1h, and then washed with hot water at 40 ℃ for one more hour. Finally, the dialysis bags were immersed in 100 mL of the simulated body fluid for 2h in order to stabilize them. This simulated medium was Phosphate Buffered Saline (PBS), pH 7.4, used as the drug release media to simulate normal blood/tissues conditions [48]. The silica samples with the adsorbed drug (0.1 g) were placed into pretreated dialysis bags with 2 mL of release media. The sealed dialysis bags were put into bottles and then 100 mL release media were added and shaken at 100 rpm at 37 ℃ under sealed conditions. The concentrations of the released drug were calculated using the Lambert-Beer law according to the absorbance of the release media at 247nm UV-Spectrometry (JASCO V-630), which is the characteristic adsorption wavelength for the methylprednisolone sodium succinate molecule.

2.4 Cell culture and viability assay

Breast cancer cells MDA-MB-231 were seeded at 30% confluence, in DMEM (Dubelcco Modified Eagle's Medium) supplemented with 10% fetal calf serum, 2 mM L-glutamine, 100 U mL^{-1} penicillin, 100 μ g mL^{-1} streptomycin at 37 ℃ in a 5% CO_2/95% O_2 and 90% RH humidify atmosphere.

MDA-MB-231 cells were transferred to 96-well plates (5000 cells per well) and allowed to attach and grow up to approximately 70 % confluence. After incubation, the old media was removed, cells were washed and new media containing pure and functionalized SBA-15 silica materials with different composition (10, 25 and 50 μg mL^{-1}) in serum free DMEM media were added. After incubation for 72 h, 4-[3-(4-iodophenyl)-2-(4-nitrophenyl)-2H-5-tetrazolio]-1,3-benzene disulfonate (WST-1 reagent) was added to the cells and further incubated for 3 h; after which, the 96-well plate was analysed at a 430 nm wavelength in a Varioskan plate reader (Thermo Scientific, Logan UT) to determine cell viability. Here, the control group was the cell media only in the absence of particles.

2.5 Characterization techniques

XRD patterns were recorded in a Phillips X'PERT MPD diffractometer equipped with a Cu-Kα source. Small angle measurements were performed in a 2θ range from 0.5 to 5°.

N_2 adsorption–desorption isotherms at 77 K were obtained in a Micromeritics Tristar 3000 sorptometer. Surface area was calculated by using the B.E.T. equation (P/P_o from 0.05 to 0.20) and the pore size distribution was obtained from the adsorption branch by means of the B.J.H. model assuming a cylindrical geometry of the pores. Degasification step prior to adsorption analyses was carried out under a nitrogen flux of 100 mL min^{-1}, at a temperature of 200 °C for pure silica SBA-15 and at 150 °C for organic-containing samples.

Thermogravimetric analyses were performed under air atmosphere with a Star system Mettler Thermobalance in the temperature range from 40 to 700 °C at 5 °C min^{-1}.

A NanoPlus DLS Zeta Potential from Micromeritics was used for obtaining the zeta potential values of the particle suspensions. The samples were suspended in Phosphate Buffered Saline (PBS) with 0.5 mg mL^{-1} concentration.

Structural characterization was completed by transmission electron microscopy (TEM) on a PHILIPS TECNAI-10 electronic microscope operating at 200 kV.

The nitrogen content, corresponding to the amino groups incorporated, was measured by elemental microanalysis on a CHNOS model Vario EL III of Elemental Analyses System GMHB.

NMR measurements, including one-dimensional (1D) single-pulse ^{29}Si MAS NMR experiments, were performed on a Varian Infinity 400 MHz spectrometer fitted with a 9.4 T magnetic field. At this field strength, ^{29}Si nuclei Larmor frequencies is 79.41 MHz. Samples were packed in 7.5 mm zirconia rotors and experiments were conducted at room temperature under MAS conditions of 6 kHz using an H/X double-resonance 7.5 mm MAS probehead. ^{29}Si MAS single-pulse experiments had 3.5 μs π/2, 3000 transients, and recycle delay time of 60 s. ^{29}Si chemical shifts were externally referenced to tetramethylsilane.

3. Results and discussion

3.1 Raw Mesoporous Silica Materials

In this work, ten different mesoporous silica materials have been employed as drug carriers: SBA-3, MCM-41, MH, SBA-16, LP-FDU-12, SBA-15, PHTS, LP-SBA-15, MCF, ULP-SBA-15. These materials have been synthesized using different methods with ionic and nonionic surfactants. Figure S1 (SI) shows their XRD patterns. Samples with 2D structures (SBA-3, MCM-41, MH, SBA-15, PHTS, LP-SBA-15, MCF and ULP-SBA-15) display the typical low-angle diffraction pattern of hexagonal *p6mm* symmetry with reflections ascribed to (100), (110) and (200) diffractions. In the case of the cubic LP-FDU-12 material, diffraction peaks at (111) and (311) ascribed to a 3D *Fm3m* structure are observed [49], while in the case of the cubic SBA-16-type sample, diffractions peaks at (110) and (200) are attributed to the well-defined 3D *Im3m* structure. Respecting the hexagonal materials, the relative position of the diffraction peaks was shifted to

lower 2-theta angles as the pore size was increased (from SBA-3, MCM-41 and MH to large-pore materials SBA-15 and LP-SBA-15). Even the patterns were less well resolved in the case of the MCF and ULP-SBA-15 silica materials, indicating an increase of the unit cell size and pore size.

TEM images of the silica samples are shown in Figure S2. The micrographs confirm the ordered *p6mm* hexagonal structure of mesostructure materials with different distances between the porous layers (SBA-3, MCM-41, MH, SBA-15, PHTS, LP-SBA-15 and ULP-SBA-15 samples). The TEM images also confirm a highly ordered mesoporous materials with three–dimensional (3-D) cage-type pores (SBA-16 and LP-FDU-12). It is important to notice that the ULP-SBA-15 experiments a great pore size increment, exhibiting a singular cylindrical mesoporous structures with hemispherical and closed end, due to the severe synthesis conditions (Fig. S2j).

The nitrogen adsorption and desorption isotherms and pore size distribution of the synthesized materials are shown in Figure S3. The isotherms corresponding to SBA-15, LP-SBA15 and ULP-SBA-15 samples are of type IV according to the IUPAC classification, with H1 hysteresis loops, characteristic of SBA-15-type mesoporous materials [50]. Higher relative pressures of hysteresis loops (LP-SBA-15, ULP-SBA-15 and MCF samples) are associated with structures of large pore diameter (Fig. S3). The isotherm of PHTS sample shows a one-step capillary condensation in the adsorption branch, indicating the filling of the uniform mesopores. However, PHTS exhibits a two-step desorption assigned to the open mesopores and plugged pores, as described in literature [51]. The isotherm for the SBA-3 silica material does not show a hysteresis loop between the adsorption and desorption branches, and it is explained as the superposition of type I (for micropores) and type IV (for mesopores) isotherm, as stated in the literature [43]. The enlarged hysteresis loop observed for the LP-FDU-12 and SBA-16 type materials is attributed to the formation of interconnected mesoporous through pore windows smaller than the size of spherical cavities [52].

Textural properties of the silica materials are included in Table 1. Different methods and ionic and nonionic surfactants were employed to obtain the purely siliceous materials. As a result of these different synthesis conditions, mesoporous silica materials with a wide range of textural properties were obtained. Thus, MCM-41, SBA-3 and MH materials were synthesized using as surfactant cationic CTAB, which supplied smaller pore sizes (28, 18 and 22 Å, respectively) with higher BET surface (1056, 1422 and 752 m^2 g^{-1}); meanwhile SBA-15 (and his pore-expanded related LP-SBA-15 and ULP-SBA-15), PHTS and MCF silicas were synthetized using non- ionic triblock copolymer P123, leading to materials with higher pore diameters. Large-pore and ultra-large-pore expanded SBA-15, LP-SBA-15 and ULP-SBA-15, were synthesized by adding 1,3,5-triisopropylbenzene as an organic swelling agent obtaining a remarkable pore sizes (130 and 300 Å) with different BET surface (730 and 388 m^2 g^{-1}). Notice the analogous BET surface area obtained for LP-SBA-15 silica material in comparison with its partner SBA-15 despite the pore size changes considerably. This fact could be provoked by the reduction in the synthesis time [53]. The swelling agent used for MCF material was 1,3,5-trimethylbenzene obtaining pores size of 110 Å with surface area of 640 m^2 g^{-1}. PHTS consists of hexagonally ordered mesopores in thick pore walls (3–6 nm) perforated with micropores, making PHTS a combined micro- and mesoporous material. In addition, PHTS possesses microporous amorphous nanoparticles (plugs) in the uniform mesoporous channels that yields higher micropore volumes. Finally, SBA-16 and LP-FDU-12, with cubic structures, were synthesized using acidic triblock copolymer F127. LP-FDU-12 presents a cubic mesostructure with a large cavity size of 123 Å and BET surface of 433 m^2 g^{-1}, while SBA-16 has a body-centered cubic structure with pore sizes of 65.2 Å and BET surface of 858 m^2 g^{-1}.

The Zeta potential values of the pure silica particles, measured at pH = 7.4, were also summarized in Table 1. As observed, all the samples exhibit negative values. This can be easily understood considering the abundancy of silanol groups onto the surface of the particles.

Table 1. Textural properties of the synthesized materials

Material	Structure	S_{BET} ($m^2 \cdot g^{-1}$)	V_p[a] ($cm^3 \cdot g^{-1}$)	D_p[a] (Å)	Z-Potential (mV) pH 7.4
SBA-3	2D hexagonal	1422	0.65	18	-10.8
MCM-41	2D hexagonal	1056	0.87	28	-16.1
MH	2D hexagonal	752	0.64	22	-10.3
SBA-16	3D cubic	858	0.66	65	-8.85
LP-FDU-12	3D cubic	433	0.60	123	-15.5
SBA-15	2D hexagonal	743	1.09	83	-15.9
PHTS	2D hexagonal	598	0.62	63	-12.6
LP-SBA-15	2D hexagonal	730	1.22	130	-13.8
MCF	3D structure	640	2.33	264	-13.9
ULP-SBA-15	2D hexagonal	388	0.78	300	-12.4
Methylprednisolone	-	-	-	-	-23.0

[a] Total pore volume and pore size as calculated by the BJH method from the adsorption branch of the N_2 isotherm

3.2 Functionalized Mesoporous Silica Materials

The surface of the synthesized silica supports were modified by incorporating 1-[3-(trimethoxysilyl)propyl]diethylenetriamine (DT) following a grafting procedure. As expected, DRX patterns after functionalization of the mesoporous silica materials reflected that the 2D and 3D structures were retained (not shown). Likewise, TEM images confirmed the well-ordered hexagonal and cubic mesostructures after functionalization by post-grafting with DT amino moieties (not shown). As a representative, ^{29}Si MAS RMN spectra of the amino-functionalized SBA-15 material (Figure S4) assessed the organosilane incorporation since a new signal attributed to DT amino group appeared at -64 and -70 ppm, assigned to T^2 and T^3, respectively. The appearance of this new signal and the simultaneously weakened Q^3 and Q^2 signals indicated that DT groups were successfully functionalized on the surface of the rehydroxylated mesoporous SBA-15 material.

Textural properties, Zeta potential values and nitrogen content of amino functionalized samples were summarized in Table 2. The incorporation of amino moieties remarkably reduced the textural properties as consequence of their attachment to the inorganic silanol groups of the silica surface. This decrease was especially pronounced in the case of the SBA-15-10DT, MCM-

41-10DT and MCF-10DT samples, where the surface area diminished from 743 to 371 $m^2 \cdot g^{-1}$ in SBA-15, from 1056 to 433.2 $m^2 \cdot g^{-1}$ in MCM-41 and from 640 to 272 $m^2 \cdot g^{-1}$in MCF. However, this fact did not cause a pore blocking in these samples, since the pore volume remained still high. In contrast, samples like SBA-3-10DT, MH-10DT and PHTS-10DT exhibited a pore volume lower than 0.2 $cm^3 \cdot g^{-1}$. The SBA-16-10DT was specially remarkable since exhibited the lowest pore volume with only 0.1 $cm^3 \cdot g^{-1}$, and experienced the greatest reduction of BET surface area from 858 to 86 $m^2 \cdot g^{-1}$, after functionalization.

Table 2 also summarizes some properties characteristic of the functionalization process, such as the efficiency in organic incorporation, nitrogen content and Zeta potential values. To check the effect of anchored amino groups on the surface charges of pure silica supports, Zeta potential of the different silica materials, functionalized and non functionalized with DT, was measured. Interestingly, the chemical modification of pure silica with DT molecule resulted in a drastic change in the surface charges and the Zeta Potential value shifted from negative (Table 1) to positive values (Table 2) for all synthetized materials. This high positive value reflects the positively charged surface of the modified silica containing basic nitrogen groups. A high zeta potential value also confers a higher electrostatic interaction between drug molecule (-23.0 mV) and modified silica materials. The obtained results also confirm the successful covalent bond of the silanol groups with the grafted DT-group in the modification process. The total DT content (showed as yield of incorporation) was assessed by means of thermogravimetric analysis, assigning the weight lost between 100 and 700 ℃ to the thermal decomposition of DT molecule. Notice the high incorporation of the functionality in samples with lower organic molar ratio (10%), comprised between 89-99 % of yield of incorporation. The nitrogen content was determined via elemental analysis and the obtained results were in agreement with the measurements of the Zeta potential values.

Table 2. Textural and superficial properties of the amino-modified mesoporous silica materials.

Material	S_{BET} ($m^2.g^{-1}$)	V_p[a] ($cm^3.g^{-1}$)	D_p[a] (Å)	Z-Potential (mV) pH 7.4	N Content [b] ($mmolN/g_{MAT}$)	Yield Organic Content [c] (%)
SBA-3-10DT	371	0.19	11.4	13.9	4.43	98.4
MCM-41-10DT	433	0.41	21.0	13.2	4.40	97.8
MH-10DT	168	0.16	21.6	10.3	4.00	88.9
SBA-16-10DT	86	0.11	58.1	13.6	4.40	97.8
LP-FDU-12-10DT	110	0.25	82.5	10.3	4.00	88.9
SBA-15-10DT	371	0.62	70.0	13.3	4.43	97.8
SBA-15-30DT	263	0.50	65.0	15.7	5.50	65.0
PHTS-10DT	112	0.17	55.6	12.8	4.26	94.7
LP-SBA-15-10DT	259	0.68	98.4	13.8	4.48	99.6
LP-SBA-15-30DT	187	0.50	93.2	14.2	4.90	74.0
MCF-10DT	272	1.32	207	12.9	4.22	93.8
MCF-30DT	196	0.97	159	13.6	5.21	69.0
ULP-SBA-15-10DT	84	0.30	280	12.9	4.28	95.1

[a] Total pore volume and pore size as calculated by the BJH method from the adsorption branch of the N_2 isotherm [b] Nitrogen content determined via elemental analysis. [c] Organic content determined via weight loss by TGA in the range 100-700 ºC

3.3. Adsorption on Raw Mesoporous Materials

The equilibrium of adsorption of methylprednisolone sodium succinate for all silica supports was measured at 298 K (Figure 1.a). In all cases, the resulting experimental adsorption isotherms showed a marked nonlinear concave shape, proving their favorable behavior, i.e. the affinity between adsorbate and adsorbent surface. Four different isotherm models were used to fit the experimental data.

Langmuir isotherm (eq. 1) is based on the assumption that adsorption takes place on a monolayer where all adsorption sites on the surface are energetically equivalent and no interaction between neighbor adsorbed molecules occurs [54].

$$q = \frac{Q_m \cdot b \cdot c}{1 + b \cdot c} \qquad \text{(eq. 1)}$$

Freundlich isotherm (eq. 2) is a semiempirical model where the adsorption sites follow an exponential decay energy distribution function [55]. Dislike Langmuir equation, Freundlich model does not describe the surface saturation with the monolayer and the linear Henry's equilibrium at low surface coverage.

$$q = K_F \cdot c^n \qquad \text{(eq. 2)}$$

To overcome the above limitations, many empirical isotherm models have been developed. Among them, Sips [56] (eq. 3) and Redlich-Peterson [57] (eq. 4) isotherms were used in the present work.

$$q = \frac{Q_m \cdot (b \cdot c)^n}{1 + (b \cdot c)^n} \qquad \text{(eq. 3)}$$

$$q = \frac{Q_m \cdot b \cdot c}{1 + (b \cdot c)^n} \qquad \text{(eq. 4)}$$

The experimental data from each adsorption equilibrium were fitted to the above four models through non-linear regression using the Levenberg-Marquardt optimization algorithm. Table S1 shows the fitting parameters corresponding to the adsorption isotherm of methyl prednisolone sodium succinate on pure mesoporous silica materials. Although the two-parameter Langmuir isotherm yielded reasonably well-fittings to all pure silica materials, both Sips and Redlich-Peterson models showed to be better suited to explain the experimental equilibrium data. In all cases, Freundlich isotherms gave the poorest results. Although fittings to Sips and Redlich-Peterson isotherms showed similar correlation coefficients closer to 1 within the experimental range studied, the maximum adsorption capacity parameter (Q_m) for Sips model agreed better with the value of the experimental asymptotic plateau observed (Figure 1.a)). Furthermore, this model allowed us to estimate the maximum drug uptake values. In Figure 1.a, the corresponding isotherms are represented as the amount methylprednisolone sodium succinate adsorbed per weight material, w_{drug}/w_{MAT}, as a function of the equilibrium concentration of methylprednisolone sodium succinate in water solution, C_{eq}. The isotherms reveal remarkable differences in adsorption capacity between the materials, although no clear dependency of loading degree on the pore diameter was observed for the materials. Hence, recalculating the methylprednisolone sodium succinate adsorption data related to the unit of specific BET surface

area, the pore size was proved to be the most relevant textural property to explain the drug adsorption effect on the raw mesoporous silica material. Thus, the amount of methylprednisolone sodium succinate adsorbed per unit specific surface area (BET) was replotted versus the equilibrium concentration, C_{eq} (Figure 1.b). The materials may be divided into three groups depending of their respective pore sizes. SBA-3, MCM-41 and SBA-16 exhibited plateau values ranged between 0.05-0.08 $mg_F.m^{-2}$. An intermediate group composed by MH, LP-FDU-12, SBA-15, PHTS and MCF displayed values plateau between 0.18-0.24 $mg.m^{-2}$, and finally the third group composed by LP-SBA-15 and ULP-SBA-15 showed values plateau between 0.28-0.34 $mg.m^{-2}$. To correlate the maximum adsorption capacities and the supports pore size, the maximum drug adsorption capacities obtained from Sips model versus pore diameter on pure silica materials was plotted (Figure S5). The results indicated that drug adsorption ability improved as the material pore size increased. Moreover, it was observed that the drug adsorption on materials with mesoporous size higher than 10 nm were very close to the theoretical saturation capacity (Table S1).

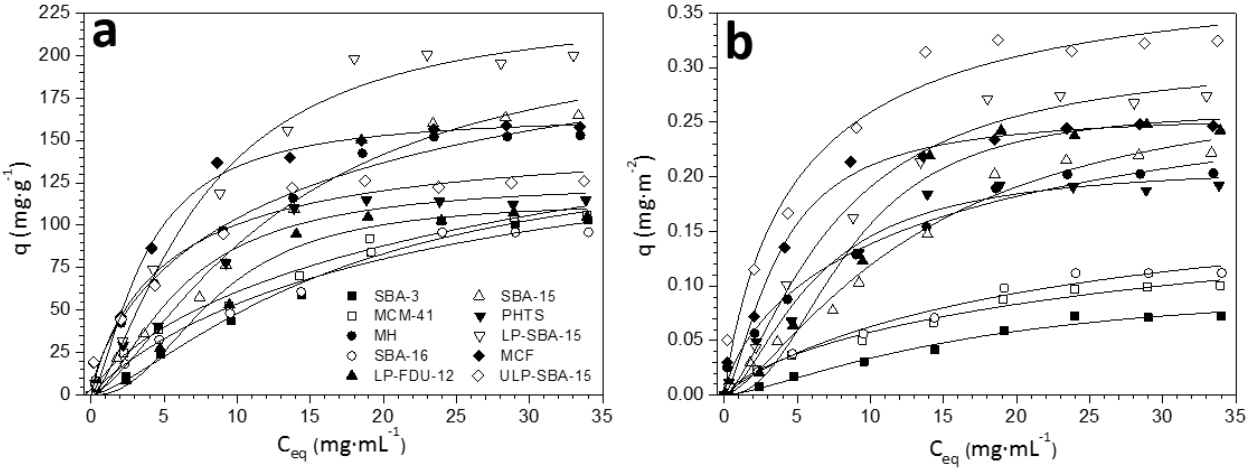

Figure 1. Experimental adsorption isotherms (symbols) and their corresponding fitting model to Sips equation (lines) for the adsorption of methylprednisolone sodium succinate onto pure silica materials (a) per unit of weight material and (b) per unit specific surface area (BET).

The selected drug loading concentration for this study and for the subsequent release kinetic experiments was 15 mg L^{-1}. Table 3 summarizes the amount of methylprednisolone sodium succinate adsorbed per unit of gram of material and per unit of BET surface area, and the pore size of the different pure silica supports.

Tabla 3. Amount of adsorbed drug over the pure silica materials

Material	D_P (Å)	Adsorbed drug ($mg \cdot g^{-1}$)	Adsorbed drug/S_{BET} ($mg \cdot m^{-2}$)
SBA-3	18	59	0.041
MCM-41	28	70	0.066
MH	22	116	0.154
SBA-16	65	61	0.071
LP-FDU-12	123	95	0.219
SBA-15	83	109	0.147
PHTS	63	110	0.184
LP-SBA15	130	156	0.214
MCF	264	140	0.219
ULP-SBA15	300	122	0.314

To better understand the corticoid drug adsorption behavior on mesoporous pure silica materials, the relationship between the textural properties and the experimental adsorption capacities were studied. The pore diameter of the silica host material determines the accessibility of the drug to the adsorption sites. Considering the results showed in Table 3 and Figure 1.b, it can be concluded that the materials with the higher values of pore diameter (LP-SBA-15, ULP-SBA-15 and MCF samples) incorporate higher drug cargos, while materials with lower pore diameters, such as SBA-3, MCM-41, SBA-16 and MH silica materials, have inferior values of drug incorporation. An exception is the helical silica material (MH), in which the helical and lengthened morphology of the particle allow for retaining higher drug amount. Furthermore, it is observed that apparently the 2D hexagonal mesoporous silica materials exhibit better capacity of drug adsorption than the 3D cubic mesostructures materials (SBA-15 vs SBA-16 and LP-FDU-12 vs LP-SBA-15). However, if the adsorbed amount of methylprednisolone sodium succinate is divided by the specific BET surface area (adsorbed drug/S_{BET} **)** the results obtained indicate that this new parameter depends only on the pore size

of the support, but not on the type of 2D or 3D structure. Figure 2 displays the relation between the amount of adsorbed drug per unit of BET surface area and the pore size of the supports. Materials with microporous and lower mesoporous size (SBA-3, MCM-41) have steric impediments to penetrate the drug molecules into the pores leading to a low adsorption performance. At intermediates, mesoporous size (SBA-15 and PHTS), the steric hindrances are not observed. In the case of 3D cubic SBA-16, even though its high mesoporous size it seems that the drug diffusion is limited since the tortuous and interconnected channels exert adverse effects to adsorb large amount of drug molecules. Finally, the materials with mesoporous channels size higher than 10 nm (LP-FDU-12, LP-SBA-15, MCF, ULP-SBA-15) enough pore space for the entrance and molecular diffusion and transportation of methylprednisolone independently of the 2D or 3D mesostructures (Figure 2).

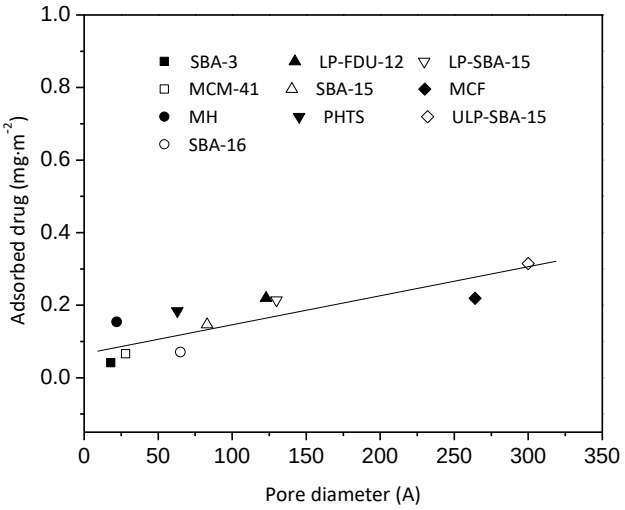

Figure 2. Amount of adsorbed drug per unit of BET surface area versus pore diameter for the raw mesoporous materials.

3.4. Adsorption on Functionalized Mesoporous Materials

The adsorption isotherms of methylprednisolone sodium succinate on amino-modified silica materials are shown in Figure 3.a. As in the case of pure silica materials, the adsorption

isotherms display a nonlinear concave shape. These experimental data were fitted using the same four models as in the case of raw mesoporous materials: Langmuir, Freundlich, Sips and Redlich-Peterson models (Table S.2). Regardless of the fit model, the maximum adsorption capacity (Q_m) was higher after surface modification evidencing an increase in the number of adsorption sites. The best fits were obtained for the Sips model in all cases. Parameter b in Sips model is related to adsorption affinity between corticoid and adsorption sites, while parameter n increases as surface heterogeneity increases [58]. It was observed that, after modification with amino groups, parameter b increased for all silica materials (except for ULP-SBA15, that remained approximately constant), which agrees well with the observed change in Z-potential after amino functionalization (Tables 1 and 2), proving the stronger interaction of methylprednisolone sodium succinate with amino groups compared to that showed for non-functionalized silica surfaces. The increase in the values of parameter n, for Sips model, evidenced the induced heterogeneity of the amino-modified silica surfaces. Figure 3.b displays the amount of methylprednisolone sodium succinate adsorbed per unit specific surface area (BET) versus the equilibrium concentration, C_{eq}. In this case, the samples can be divided in two groups. SBA-3-10DT, MCM-41-10DT, SBA-15-10DT, MCF-10DT, LP-SBA-15-10DT and MH-10DT exhibited values plateau between 0.05-2 mg $\cdot m^{-2}$ while PHTS-10DT, LP-FDU-12-10DT, SBA-16-10DT and ULP-SBA-15-10DT between 4-5.8 mg $\cdot m^{-2}$. Consequently, these results do not give any satisfactory information about the adsorption process.

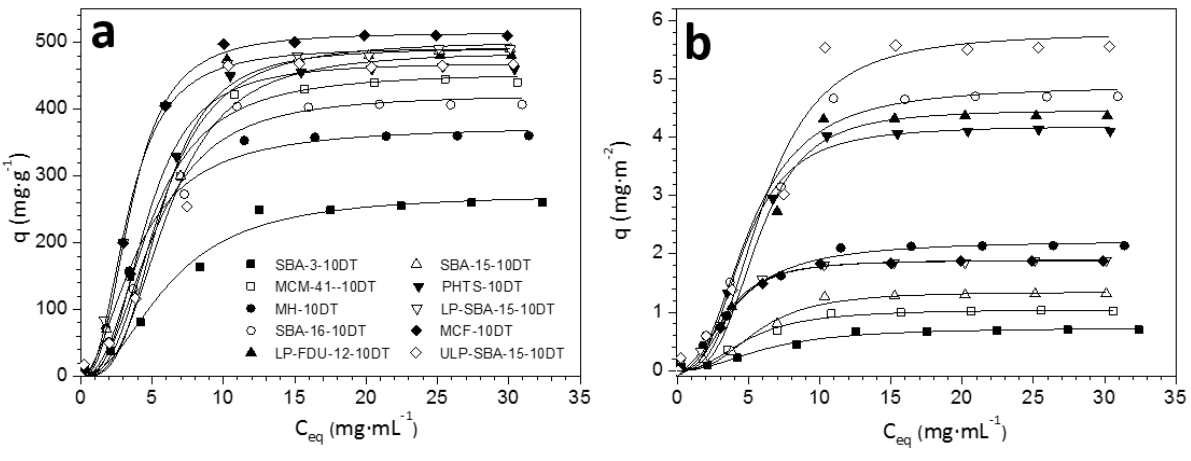

Figure 3. Experimental adsorption isotherms (symbols) fitted to Sips model equation (lines) for the adsorption of methylprednisolone sodium succinate onto amino-modified silica materials (a) per unit of weight material and (b) per unit specific surface area (BET).

As in the case of raw silica samples, the selected drug loading concentration for this study and for the subsequent release kinetic experiments was 15 mg L^{-1}. Thus, for this condition, Table 4 summarizes the drug adsorbed per unit of gram of material and per nitrogen content for the different functionalized silica materials. With regard to the drug adsorption data on the DT amine-modified mesoporous materials, it is observed that functionalized samples show higher drug loads than the non-functionalized mesoporous silica supports. This result correlates well with the stronger attractive electrostatic interactions between methylprednisolone and the amino-silica surfaces. Zeta potential measurements show that the amino-modified surfaces of the mesoporous silica materials have an overall positive charges, opposite to the raw mesoporous silica material that present negative ones. Bearing in mind the high negative zeta potential that methylprednisolone possesses (-23.0 mV), these species will be more electrostatic attracted to, and therefore more adsorbed to, the positive DT amino-functionalized silica surface. Thus, after grafting DT amino groups a vast amount of drug was incorporated into the mesoporous silica hosts. However, this is not the only factor that controls the methylprednisolone species adsorption into the silica hosts, since although the raw silica materials have negative surfaces, it is able to adsorb a remarkable amount of

methylprednisolone species. An explanation was previously reported by our group, taking into account the attractive hydrogen-bonding and/or hydrophobic interactions as factors to be considered synergetic together with the electrostatic interactions on the ability of the mesoporous silica materials to adsorb methylprednisolone moieties [24].

Tabla 4. Amount of adsorbed drug over the amino-modified silica samples.

Material	D_P (Å)	Adsorbed drug ($mg \cdot g^{-1}$)	Adsorbed drug/N content ($mg \cdot mmol\ N^{-1}$)	mol_{drug}/mol_{DT}	q_m ($mmol_{drug} \cdot m^{-2}$)	q_m ($mmol_{DT} \cdot m^{-2}$)
SBA-3-10DT	11.4	249	56.2	0.53	0.002	0.004
MCM-41-10DT	21	421	95.7	0.82	0.003	0.003
MH-10DT	21.6	353	88.2	0.72	0.006	0.008
SBA-16-10DT	58.1	404	91.8	0.81	0.014	0.017
LP-FDU-12-10DT	82.5	474	118.5	1.04	0.013	0.012
SBA-15-10DT	70	460	103.8	0.99	0.004	0.004
PHTS-10DT	55.6	450	105.6	0.88	0.011	0.013
LP-SBA-15-10DT	98.4	469	104.7	0.85	0.005	0.006
MCF-10DT	207	500	118.5	0.92	0.005	0.005
ULP-SBA-15-10DT	280	465	108.6	1.02	0.017	0.017

Table 4 also displays the mol_{drug}/mol_{DT} ratio, as indicative of the DT molecules able to adsorb the drug molecules. Mesoporous silica materials with low pore size (SBA-3-10DT, MCM-41-10DT, MH-10DT) exhibit the poorer ratio, which means that a significant percentage of DT molecules do not interact with the drug molecules, due to the low pore size of these materials. Quite remarkable is the case of the SBA-3-10DT material, in which only the 50% of the DT molecules interact with the drug moieties. This can be explained by its microporous size, containing pores with 11.4 Å size, which hinders the access of the drug moieties to the inner porosity. Although SBA-16-10DT sample possesses an intermediate pore size, its intricate pore 3D structure could be the factor that determines its low mol_{drug}/mol_{DT} ratio, similar to the aforementioned materials with lower pore size.

Otherwise, Table 4 shows the DT molecules density values and the drug adsorbed molecules, both expressed per unit area for all the studied materials. Figure 4.a depicts practically linear fitting between these values, confirming the clear dependence of the drug adsorption respecting the amino group content.

Focusing on the textural properties, the pore diameter is also a determinant factor on the drug adsorption to the functionalized silica materials. As shown in Figure 4.b, the DT amino-modified silica materials with lower pore size present lower values of methylprednisolone adsorbed, while materials with greater pore diameter adsorbed higher amounts, although a plateau is reached upon exceeding certain pore diameter threshold, at around 100 Å. This same trend is observed when the amount of adsorbed drug per nitrogen content is shown (Table 4). SBA-3-10DT is the material with the lowest value of drug adsorbed, 249 $m^2 \cdot g^{-1}$. This fact is accounted for the molecular dimension of methylprednisolone sodium succinate longitudinally measured (1.9 nm, Scheme S1) that is higher than SBA-3-10DT pore diameter, and consequently the drug molecules suffer remarkable steric hindrances. However, it is noteworthy to emphasize the awesome capacity of drug adsorption that presents the SBA-3-10DT in comparison with its counterpart raw mesoporous silica material. Comparing materials with small and similar mesopore size, MCM-41-10DT and MH-10DT (21.0 and 21.6 Å, respectively), it confirmed that the factor governing the adsorption process was mainly the electrostatic interactions (and in lesser extension the above mentioned, hydrogen bonding and/or hydrophobic-hydrophilic interactions) between the drug moieties and amino-functionalized silica surfaces, and in a lesser degree the textural properties. MCM-41-10DT has an overall higher positive chemistry surface than MH-10DT, and as consequence exerts higher attraction over the drug molecules.

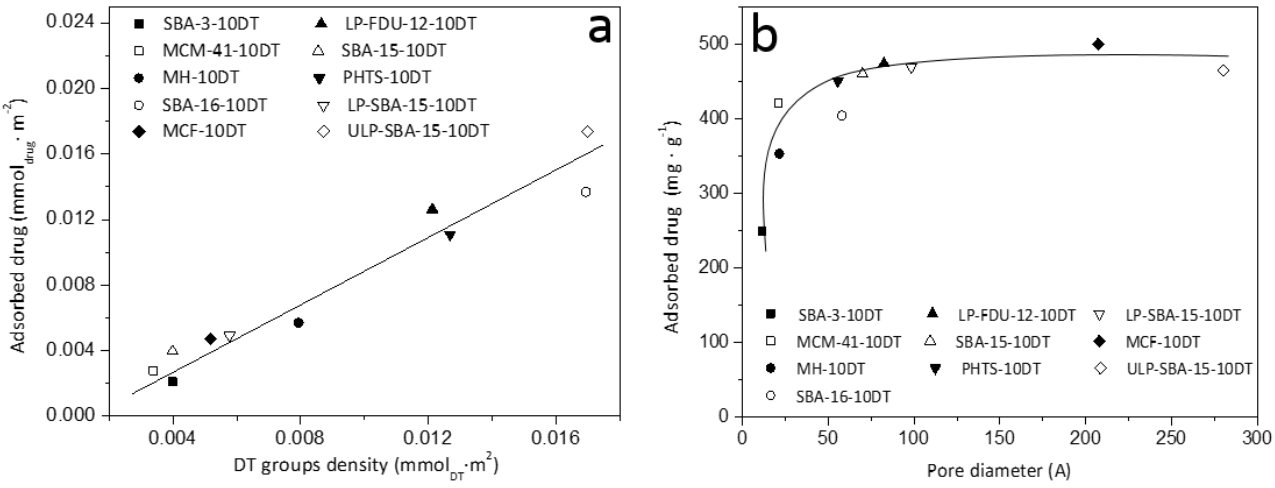

Figure 4**.** (a) Drug adsorption capacity versus DT groups density expressed per unit BET surface and (b) amount of adsorbed drug versus of pore diameter of the different amino-modified materials.

3.5 Release from raw and DT amino-functionalized silica samples

For the methylprednisolone sodium succinate released from the non-functionalized and functionalized mesoporous silica materials, the drug-loaded nanoparticles were soaked in simulated body fluids (SBF) under neutral conditions, corresponding to those in the blood stream at 37°C. The amounts of methylprednisolone species released can be estimated by using UV-visible spectroscopy to measure the absorbance intensity at 247 nm, which is associated with methylprednisolone species. The cumulative release of methylprednisolone sodium succinate from both raw and amino-functionalized mesoporous silica materials was calculated. The release percentage of the samples was plotted against the release time, and the results are shown in Figure 5 and 6 for non-functionalized and functionalized silica materials, respectively.

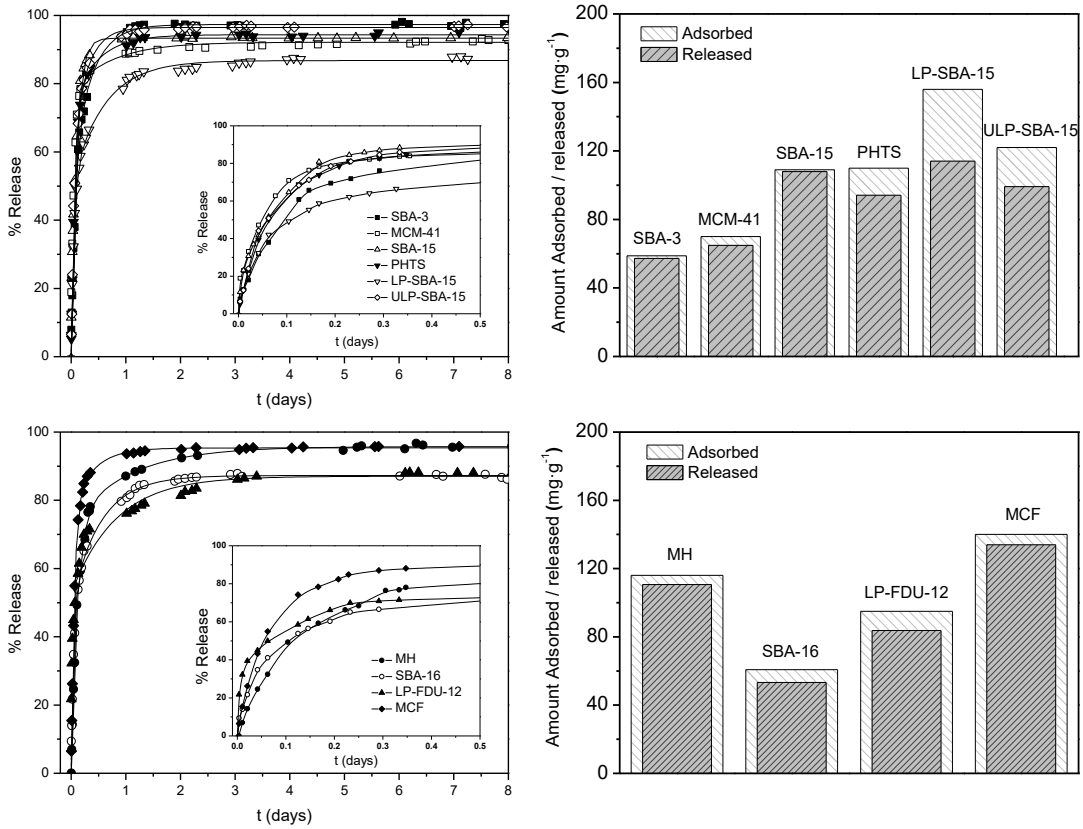

Figure 5. Methylprednisolone sodium succinate release percentages as a function of release time, using the non-functionalized mesoporous silica materials as carriers.

Understanding the kinetics of drug release from mesoporous silica carriers affords supplementary insight on designing of optimal drug delivery systems. To quantify the release rate, experimental data were fitted to three different kinetic models. The Korsmeyer-Peppas model [59] follows a power law mathematical relationship (eq. 5) between the amount of drug released and the time.

$$f(t) = K_{KP} \cdot t^{n} \qquad \text{(eq. 5)}$$

where f(t) is the cumulative drug released with respect to the mass of solid carrier over time t, and K_{KP} and n are model constants. From the correlation coefficients (r^2 within the range 0.980-0.999) for the desorption of the corticoid from both non-functionalized (Table S3) and amino modified (Table S4) silica adsorbents, it appears that the experimental data on drug release fit well to the model. For all materials, the parameter n ranged from 0.5 to 0.8, approximately,

which indicates that the release was dominated by non-Fickian diffusion, as consequence of the variable contribution of geometric pore structure characteristics as n shifts from 0.5 towards higher values [60]. These results prove that the methylprednisolone moieties diffusion processes are mediated by the interaction of the drug species within mesoporous silica channels, more pronounced in the functionalized silica adsorbents. Interestingly, the parameter n increased after DT functionalization in those silica materials (SBA-3-10DT and LP-FDU-12-10DT) where the reduction in pore diameter was higher with respect to their corresponding non-functionalized silica carrier, indicating that the drug diffusion in these DT-mesoporous materials is more impeded or restricted by the interactions among methylprednisolone moieties and the surface of amino-modified silicas. It is important to note that the Korsmeyer-Peppas model only describes the initial part of the kinetics, i.e., for f(t) values lower than 60% of the maximum cumulative drug released.

The methylprednisolone species release from non-functionalized and functionalized mesoporous silica materials was also fitted to the first-order kinetic model (eq. 6). In this simple model, the rate of drug release from the mesostructured material is proportional to the concentration of methylprednisolone in the simulated body fluid.

$$f(t) = f_{\max} \cdot [1 - \exp(-K \cdot t)] \qquad \text{(eq. 6)}$$

Thus, the release firs-order kinetic constants, K, were determined (Tables S3 and S4). Except for some non-functionalized materials (MCM-41, SBA-16, LP-FDU-12 and MCM-41-10DT) all r^2 values were above 0.980, indicating that experimental data fitted reasonably well to this model. Respecting the non-functionalized materials, analyses of the cumulative drug release profiles using the first-order kinetic model reveal that the lowest first-order rate coefficients are associated with materials that possess small pore diameters, such as SBA-3, SBA-16 and MH silica materials (7.3, 7.9 and 5.8 d^{-1}, respectively). These rate coefficients are lower than those associated with larger pore size diameter materials (for example, LP-FDU-12, LP-SBA-15, MCF

with first order release constant of 14.0, 12.1 and 12.9 d^{-1}, respectively). Remarkable exceptions are MCM-41 and SBA-15 silica materials (17 d^{-1} and 13.9 d^{-1}), these materials are characterized by the straight long cylindrical mesopores, which facilitates the drug species diffusion without serious impediments. On the contrary, the 3D cubic mesostructure in SBA-16 material displays tortuous pore channels, in addition to pore sizes more adjustable to the molecular dimension of drug species. These features hinder the molecular diffusion and transportation of methylprednisolone moieties. The slowest release rate coefficient was displayed by the MH silica material (5.8 d^{-1}), where the helical morphology likely contributes to complicate the diffusion of methylprednisolone species. Regarding the raw mesoporous silica materials with higher pore diameters, above 100 Å, the rate coefficients are higher than those obtained for smaller pore ones. Among them, the smallest constant of proportionality was obtained for ULP-SBA-15 material, which likely can be explained for its mesoporous structure with hemispherical and closed end mesopores that contribute to slow down the drug moieties release. LP-SBA-15, LP-FDU-12 and MCF present similar rate coefficients, although the latter 3D mesostructures have higher values, probably due to their large 3D interconnected channels that facilitates the faster corticoid diffusion through the silica pores.

Regarding the functionalized mesoporous silica materials, the first-order rate coefficients were also calculated from the release rate plot at low drug release concentration (Table S3) when the kinetic model is first-order with respect to the drug release amount. As previously proved, the amino functionalities at the silica surface of mesoporous silicas significantly influenced the methylprednisolone species adsorption. Likewise, the release behavior is clearly mediated by the DT amino organosilica species. Generally, analyses of the cumulative methylprednisolone release profiles (Figure S6) using the first-order kinetic model reveal a drastic decreasing in the first-order rate coefficients of amino-functionalized mesoporous materials relative to their counterpart raw silica materials. A reasonable interpretation can be based on the same electrostatic attractions (and attractive hydrogen-bonding) between adsorbates and

adsorbents. The grafting amino groups to the surface of the mesoporous materials enhance the retention of the methylprednisolone species, and therefore resulting in a more controlled and sustained delivery. Specifically, the highest first-order rate coefficient was observed for SBA-3-10DT silica material (5.27 d^{-1}), where the small pore size (11.4 Å) hinder the methylprednisolone entrance and most of drug moieties are located on the outer surface, resulting in a less favored attraction to the binding sites. Additionally, the sorption equilibrium is favored from the silica materials to the aqueous simulated body fluid since continuous influx of water is in contact with the drug species. The rest of the functionalized silica materials present constants of proportionality near or below 1.0 d^{-1} (Table S4). Methylprednisolone species are able to diffuse within the functionalized silica materials and as consequence to be stronger attracted to the binding sites. However, the textural properties and morphology particles also play an important role in the methylprednisolone controlled release. Thus, the lowest first-order rate coefficients (0.55 and 0.57 d^{-1}), are observed for materials that possess intricate helical and 3-D cubic structures, MH-10DT and SBA-16-10DT, respectively. Furthermore, despite its great pore diameter, the ULP-SBA-15-10DT material present a low kinetic constant value of 0.60 d^{-1} that is accounted for its particular morphology composed by hemispherical and closed end mesopore channels that slow down the methylprednisolone release species.

To improve the accuracy of the model predictions the Gallagher-Corrigan model [61], was used additionally to fit the experimental data. This model describes a drug release in two sequential steps showing different kinetics (eq. 7). The first step comprises a fast release ("burst effect") of non-bound to matrix or externally adsorbed drug with kinetic constant k_1 followed by a slow release characterized by a lower kinetic constant, k_2.

$$f(t) = f_{\max} \cdot \left[1 - \exp(-k_1 \cdot t)\right] + \left(f_{\max} - f_B\right) \frac{\exp(k_2 \cdot t - k_2 t_2)}{\left[1 + \exp(k_2 \cdot t - k_2 t_2)\right]} \qquad \text{(eq. 7)}$$

In all cases, the Gallagher-Corrigan model significantly increased the correlation coefficients, proving to be a more accurate model describing the experimental data. It was observed (Tables S3 and S4) that the kinetic constant of the initial burst step (k_1), decreased after DT-functionalization, showing that amino-modification of silica mesoporous silica carriers is a satisfactory strategy towards efficient and reliable design of drug release systems.

Based on the cumulative fractions of methylprednisolone released from the non-functionalized silica materials depicted in Figure 5, it is inferred that drug moieties were delivered at times lower than 2-3 days. Moreover, the fractions of drug species released from these materials were in all the cases higher than 85 %, and for some materials such as SBA-3 and SBA-5 near to 100 %. These results indicate almost complete methylprednisolone release, excepting the LP-SBA-15 and ULP-SBA-15 probably due to sorption equilibrium of methylprednisolone species with the mesoporous silica surfaces. Figure 6 shows the results for functionalized silica materials, and comparatively lower fractions of drug moieties were released from these materials (~75-95%). The drug moieties were released at times clearly higher than those of the counterpart raw silica materials, and even exceeding 8-9 days. Moreover, remarkable lower rates of methylprednisolone release were observed for DT amino-functionalized silica materials, compared to non-functionalized mesoporous SBA-15 silica materials, which is accounted for the stronger electrostatic interactions (and hydrogen-bonding interactions) that provide the DT amino-modified silica surface, resulting in a more attraction to these binding sites, and therefore slowing down the methylprednisolone species release.

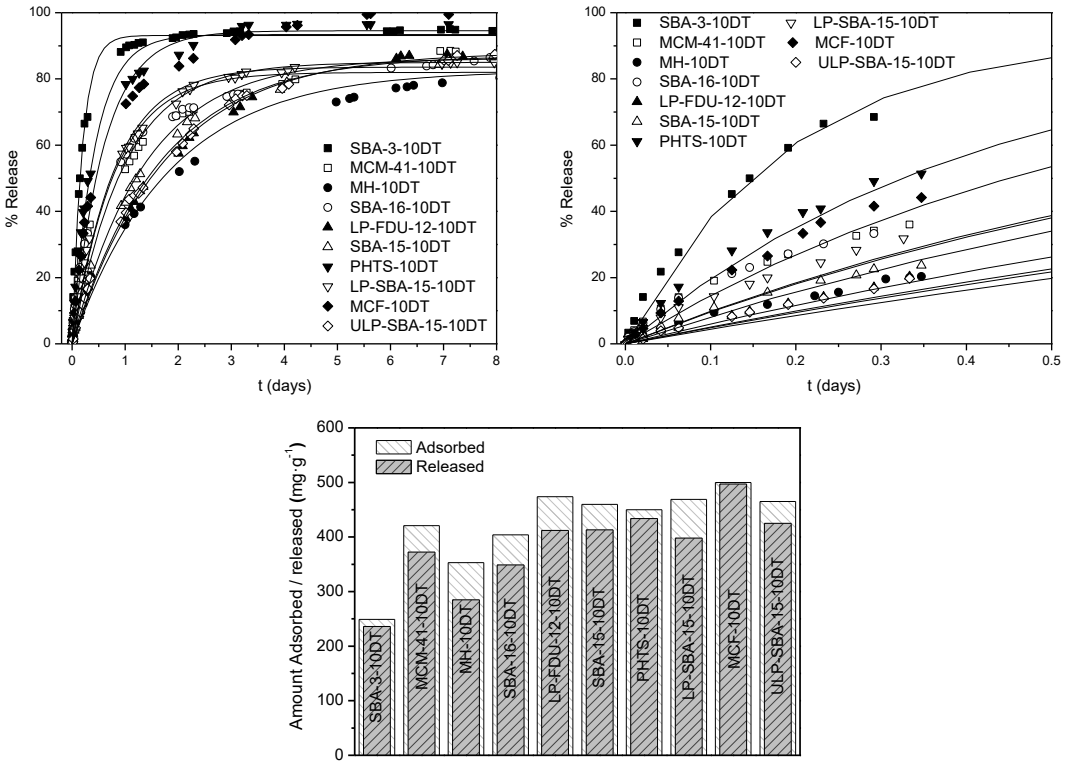

Figure 6. Methylprednisolone sodium succinate release percentages as a function of release time, using the amino modified mesoporous silica materials as carriers.

3.6 Drug loading and release over mesoporous silica materials modified with 30DT

According to the results above commented in previous sections, the silica materials functionalized with molecules containing DT group have shown to be particularly effective in the drug controlled administration. For this reason, the mesoporous silicas inner surfaces were modified adding 30 % molar ratio of DT amino organosilane relative to silica, instead the 10% previously used. With this modification, it is pursued increasing the amount of amino species covering the silica surface to more efficiently control the drug delivery. The chosen silica materials to be modified with DT organosilane in 30 % molar ratio were SBA-15, LP-SBA-15 and MCF, based on that these materials evidenced a lower BET surface area decrease at 10 % molar ratio of DT amino species. Thus, the remarkable 50, 35 and 43 %, respectively, of the surface area remained free after the anchoring of amino moieties. The new synthesized materials were

denoted as SBA-15-30DT, LP-SBA-15-30DT and MCF-30DT. Pore size, BET surface area and pore volume values of these materials were also summarized in Table 2.

Analyses of N_2 adsorption data reveal a significantly reduced BET surfaces areas for 30DT functionalized materials (263, 187 and 196 m^2g^{-1}, respectively) which results from the added mass associated with grafted amino-organosilica species, resulting in a 35, 26 and 31 %, respectively, of free inner silica surface after addition. The pore volumes of amino-modified materials (0.5 cm^3g^{-1} for SBA-15-30DT and LP-SBA-15-30DT) resulted remarkably lower than the corresponding raw silica, indicating the successful amino-organosilane incorporations. The quantities of amino-organosilanes species grafted to the surface of silica in terms of nitrogen content were obtained by using elemental analysis, and represented in Table 2. From this analysis, it was established a yield organic content into silica of 65, 74, and 69 % respecting the theoretical initial amount added. These results were lower than those of the functionalized silica materials with 10% molar ratio (97.8, 99.6 and 93.8, respectively), and evidence that there are no free silanols to react with the organosilanes or the access to the silanol sites are impeded.

The methylprednisolone release percentages from non-functionalized and functionalized SBA-15, LP-SBA-5 and MCF amino materials with 10 and 30 % DT amino species were quantified and analyzed to understand how amino moieties influence the drug release behaviors (Figure 7 (a) for SBA-15, (b) for LP-SBA-15, (c) for MCF materials). Interestingly, there are no differences between the release curves observed for 10DT and 30DT LP-SBA-15 materials, since the adsorbed drug was similar for both materials (469 vs 480 $mg{\cdot}g^{-1}$). Moderate differences in the release behaviors of methylprednisolone species from SBA-15-30DT and MCF-30DT materials were observed compared to the 10DT ones, which means that the drug species release is mediated by the amount of anchored amino species at the mesoporous surface. For both materials, the higher nitrogen content correlates well with the larger drug adsorption into and slower drug release from the functionalized materials. These results can be explained by the

stronger interactions of methylprednisolone species with the diethylentriamine grafted to the materials. Moreover, analyses of the instantaneous release profiles of SBA-15-30DT, LP-SBA-15-30DT and MCF-30DT materials using a first-order kinetic release model (Table S4) yields first-order rate coefficients of 0.56, 1.11 and 0.92 d^{-1}, respectively. These rate coefficients are lower than those associated with 10 % DT functionalized materials, establishing the slower release of methylprednisolone from mesoporous silica materials with higher amino surface functionalities.

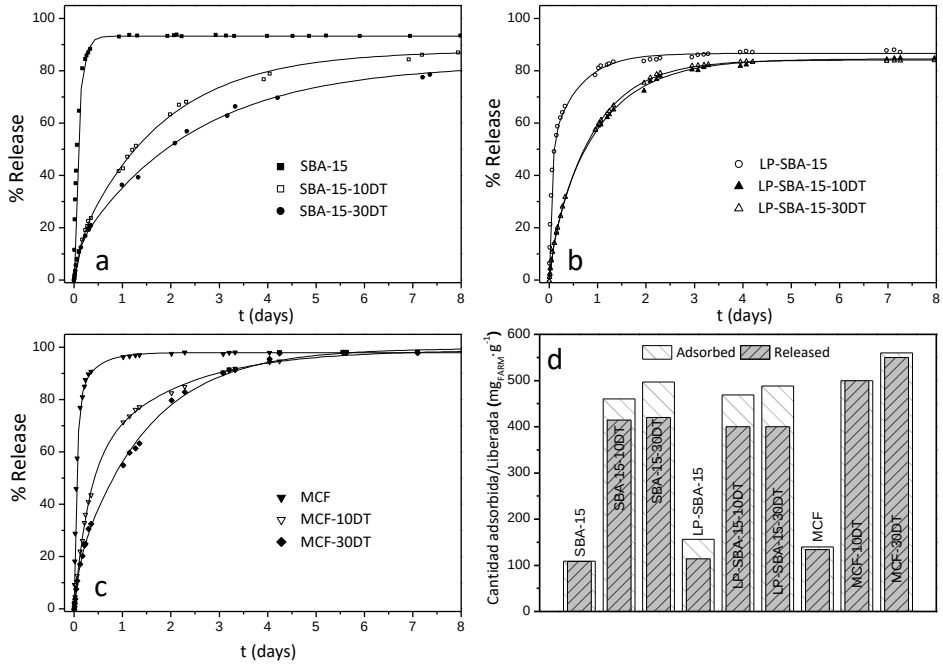

Figure 7. Methylprednisolone sodium succinate release percentages as a function of release time, using (a) SBA-15 materials, (b) LP-SBA-15 materials, (c) MCF materials and (c) Amount of methylprednisolone sodium succinate adsorbed and released in 8 days by the selected pure and amino modified mesoporous silica materials

Drug-release values after 8 days for the selected modified mesoporous silica materials are displayed in Figure 7 (d). The results show that those materials with higher drug loading correlates well with higher amount of drug released. Interestingly, the fractions of methylprednisolone released from non-functionalized and functionalized silica materials approach to values near 90 %, and in the specific case of MCF the extent of drug release is near

100 %, as shown in Figure 7 (d). This fact can be probably explained by the prevalence of relatively weak drug−drug intermolecular interactions, in opposition to the stronger drug-host interactions, that facilitates methylprednisolone release into the aqueous body fluid media. In addition, the large pore volume and pore diameter remaining in MCF materials, after their inner mesoporous surface DT amino species anchoring, facilitates the continuous influx of simulated body fluid sweeping the drug species from the silica to the aqueous media.

The synthesized samples with higher amount of amino group show a slowing in the drug release, and hence driving a more controlled *in vitro* drug administration. As conclusion, amino functionalized mesoporous silicas have been proved to be successful in establishing stronger interactions among methylprednisolone molecule and the aminosilane species that decorates the silica surface. These surface-modified mesoporous silica drug delivery vehicles allow precise control of surface chemistry to modulate the drug cargo to reach out the site specific targeting on body to be effective to fighting against the illness.

3.7 Cell viability

Finally, the *in vitro* cytocompatibility of all hybrid materials prepared was examined on cultured MDA-MB-231 Breast cancer cells adopting the WST-1 assay [62]. The cells were exposed for 72 h to the medium containing the selected mesoporous materials in the concentration range of 10-50 μg mL^{-1} (Figure S7). WST-1 assay results revealed that the mesoporous materials were not cytotoxic towards the cells (> 80% viability), although a slight decrease in cell proliferation was observed as compared to the untreated cells. These results are in agreement with previous studies [63], indicating that amino modified silica-based mesoporous materials induce no cytotoxic effects on the cells.

4. Conclusions

Ten mesoporous silica materials with different structures and with a wide range of textural properties have been successfully synthesized and functionalized with amino groups to evaluate the influence of these variables in the adsorption and *in vitro* release of the glucocorticoid methylprednisolone sodium succinate. The experimental data from adsorption equilibrium isotherm were fitted to four isotherm models: Langmuir, Freundlich, Sips and Redlich-Peterson models. In all cases, the best fits have been obtained for the Sips model. The experimental data from *in vitro* methylprednisolone release were fitted to three kinetic models: Korsmeyer-Peppas, first-order kinetic models and Gallagher-Corrigan. For all the materials, the highest correlation coefficients have been obtained for Gallagher-Corrigan model that describes the drug release in two steps with different kinetic constants. The drug adsorption capacities of the amino-modified materials were considerably higher than that of raw silica samples. Likewise, remarkable lower drug release rates were obtained for functionalized materials compared with that of non-functionalized materials. Besides, an increase in the number of amino groups incorporated into silica materials has been accompanied by an improvement in the drug adsorption capacity and a better control in the drug delivery. These results were attributed to the strong electrostatic interactions between the hydrophilic drug and the polar amino moieties also with hydrophilic character. On the other hand, respect to the effect of the different textural properties and structure of the synthesized materials, it can be concluded that the pore size is the determinant factor on the drug adsorption/desorption process. Materials with lower mesoporous size show steric impediments to the drug molecules diffusion so that lower drug adsorption performance and slower drug release rates have been observed. On the contrary, materials with higher mesoporous size have exhibited elevated adsorption performance and drug release rates, due to the sufficient space in mesoporous channel for the drug diffusion. Finally, the *in vitro* cytocompatibility experiments have revealed that all hybrid materials

prepared were not cytotoxic towards the cells for a silica concentration range between 10 and 50 $\mu g \cdot mL^{-1}$.

Acknowledgments

The financial support of the Spanish government (CTQ2011-22707, CTQ2014-57858-R) is gratefully acknowledged.

References

[1] M. Moritz, M. Geszke-Moritz, Mesoporous materials as multifunctional tools in biosciences: Principles and applications, Mater. Sci. Eng. C 49 (2015) 114-151.
[2] V. Mamaeva, C. Sahlgren, M. Linden, Mesoporous silica nanoparticles in medicine--recent advances, Adv. Drug Deliv. Rev. 65 (2013) 689-702.
[3] R.A. García-Muñoz, V. Morales, M. Linares, B. Rico-Oller, Synthesis of Helical and Supplementary Chirally Doped PMO Materials. Suitable Catalysts for Asymmetric Synthesis, Langmuir 30 (2014) 881-890.
[4] R.A. Garcia, V. Morales, T. Garces, One-step synthesis of a thioester chiral PMO and its use as a catalyst in asymmetric oxidation reactions, J. Mater. Chem. 22 (2012) 2607-2615.
[5] V. Morales, J.A. Villajos, R.A. García, Simultaneous synthesis of modified Binol-periodic mesoporous organosilica SBA-15 type material. Application as catalysts in asymmetric sulfoxidation reactions, J. Mater. Sci 48 (2013) 5990-6000.
[6] S. Wang, Ordered mesoporous materials for drug delivery, Microporous Mesoporous Mater. 117 (2009) 1-9.
[7] I. Izquierdo-Barba, M. Colilla, M. Manzano, M. Vallet-Regí, In vitro stability of SBA-15 under physiological conditions, Microporous Mesoporous Mater. 132 (2010) 442-452.
[8] X. Huang, X. Teng, D. Chen, F. Tang, J. He, The effect of the shape of mesoporous silica nanoparticles on cellular uptake and cell function, Biomaterials 31 (2010) 438-448.
[9] Q. He, J. Shi, F. Chen, M. Zhu, L. Zhang, An anticancer drug delivery system based on surfactant-templated mesoporous silica nanoparticles, Biomaterials 31 (2010) 3335-3346.
[10] Y. Zhang, H.F. Chan, K.W. Leong, Advanced materials and processing for drug delivery: The past and the future, Adv. Drug Deliv. Rev. 65 (2013) 104-120.
[11] M. Colilla, B. Gonzalez, M. Vallet-Regi, Mesoporous silica nanoparticles for the design of smart delivery nanodevices, Biomater. Sci. 1 (2013) 114-134.
[12] D.M. Schlipf, S.E. Rankin, B.L. Knutson, Selective external surface functionalization of large-pore silica materials capable of protein loading, Microporous Mesoporous Mater. 244 (2017) 199-207.
[13] V. Morales, M. Gutiérrez-Salmerón, M. Balabasquer, J. Ortiz-Bustos, A. Chocarro-Calvo, C. García-Jiménez, R.A. García-Muñoz, New Drug-Structure-Directing Agent Concept: Inherent Pharmacological Activity Combined with Templating Solid and Hollow-Shell Mesostructured Silica Nanoparticles, Adv. Funct. Mater. 26 (2016) 7291-7303.
[14] J.M. Rosenholm, M. Linden, Towards establishing structure-activity relationships for mesoporous silica in drug delivery applications, J. Control. Release 128 (2008) 157-164.

[15] P. Yang, Z. Quan, L. Lu, S. Huang, J. Lin, Luminescence functionalization of mesoporous silica with different morphologies and applications as drug delivery systems, Biomaterials 29 (2008) 692-702.
[16] G. Wang, A.N. Otuonye, E.A. Blair, K. Denton, Z. Tao, T. Asefa, Functionalized mesoporous materials for adsorption and release of different drug molecules: A comparative study, J. Solid State Chem. 182 (2009) 1649-1660.
[17] R. Mortera, S. Fiorilli, E. Garrone, E. Verné, B. Onida, Pores occlusion in MCM-41 spheres immersed in SBF and the effect on ibuprofen delivery kinetics: A quantitative model, Chem. Eng. J. 156 (2010) 184-192.
[18] J. Salonen, L. Laitinen, A.M. Kaukonen, J. Tuura, M. Björkqvist, T. Heikkilä, K. Vähä-Heikkilä, J. Hirvonen, V.P. Lehto, Mesoporous silicon microparticles for oral drug delivery: Loading and release of five model drugs, J. Control. Release 108 (2005) 362-374.
[19] A.L. Doadrio, E.M.B. Sousa, J.C. Doadrio, J. Pérez Pariente, I. Izquierdo-Barba, M. Vallet-Regí, Mesoporous SBA-15 HPLC evaluation for controlled gentamicin drug delivery, J. Control. Release 97 (2004) 125-132.
[20] Q. He, J. Shi, Mesoporous silica nanoparticle based nano drug delivery systems: synthesis, controlled drug release and delivery, pharmacokinetics and biocompatibility, J. Mater. Chem. 21 (2011) 5845-5855.
[21] P. Horcajada, A. Ramila, J. Perez-Pariente, M. Vallet-Regı, Influence of pore size of MCM-41 matrices on drug delivery rate, Microporous Mesoporous Mater. 68 (2004) 105-109.
[22] H. Hata, S. Saeki, T. Kimura, Y. Sugahara, K. Kuroda, Adsorption of taxol into ordered mesoporous silicas with various pore diameters, Chem. Mater. 11 (1999) 1110-1119.
[23] N.K. Mal, M. Fujiwara, Y. Tanaka, Photocontrolled reversible release of guest molecules from coumarin-modified mesoporous silica, Nature 421 (2003) 350-353.
[24] V. Morales, M.N. Idso, M. Balabasquer, B. Chmelka, R.A. García-Muñoz, Correlating Surface-Functionalization of Mesoporous Silica with Adsorption and Release of Pharmaceutical Guest Species, J. Phys. Chem. C 120 (2016) 16887-16898.
[25] B. Muñoz, A. Rámila, J. Pérez-Pariente, I. Díaz, M. Vallet-Regí, MCM-41 Organic Modification as Drug Delivery Rate Regulator, Chem. Mater. 15 (2003) 500-503.
[26] S. Simovic, N. Ghouchi-Eskandar, A. Moom Sinn, D. Losic, C. A. Prestidge, Silica Materials in Drug Delivery Applications, Curr. Drug Discov. Technol. 8 (2011) 250-268.
[27] A. Nieto, S. Areva, T. Wilson, R. Viitala, M. Vallet-Regi, Cell viability in a wet silica gel, Acta biomater. 5 (2009) 3478-3487.
[28] M. Cicuéndez, I. Izquierdo-Barba, M.T. Portolés, M. Vallet-Regí, Biocompatibility and levofloxacin delivery of mesoporous materials, Eur. J. Pharm. Biopharm. 84 (2013) 115-124.
[29] F.J. Trindade, G.J.T. Fernandes, A.S. Araújo, V.J. Fernandes Jr, B.P.G. Silva, R.Y. Nagayasu, M.J. Politi, F.L. Castro, S. Brochsztain, Covalent attachment of 3,4,9,10-perylenediimides onto the walls of mesoporous molecular sieves MCM-41 and SBA-15, Microporous Mesoporous Mater. 113 (2008) 463-471.
[30] I. Izquierdo-Barba, Á. Martinez, A.L. Doadrio, J. Pérez-Pariente, M. Vallet-Regí, Release evaluation of drugs from ordered three-dimensional silica structures, Eur. J. Pharm. Sci 26 (2005) 365-373.
[31] S. Zhu, Z. Zhou, D. Zhang, C. Jin, Z. Li, Design and synthesis of delivery system based on SBA-15 with magnetic particles formed in situ and thermo-sensitive PNIPA as controlled switch, Microporous Mesoporous Mater. 106 (2007) 56-61.
[32] J. Xi, J. Qin, L. Fan, Chondroitin sulfate functionalized mesostructured silica nanoparticles as biocompatible carriers for drug delivery, In. J. Nanomedicine 7 (2012) 5235-5247.
[33] Q. Yang, S. Wang, P. Fan, L. Wang, Y. Di, K. Lin, F.-S. Xiao, pH-Responsive Carrier System Based on Carboxylic Acid Modified Mesoporous Silica and Polyelectrolyte for Drug Delivery, Chem. Mater. 17 (2005) 5999-6003.
[34] C.Y. Lai, B.G. Trewyn, D.M. Jeftinija, K. Jeftinija, S. Xu, S. Jeftinija, V.S. Lin, A mesoporous silica nanosphere-based carrier system with chemically removable CdS nanoparticle caps for

stimuli-responsive controlled release of neurotransmitters and drug molecules, J. Am. Chem. Soc. 125 (2003) 4451-4459.
[35] Z. Zhou, S. Zhu, D. Zhang, Grafting of thermo-responsive polymer inside mesoporous silica with large pore size using ATRP and investigation of its use in drug release, J. Mater. Chem. 17 (2007) 2428-2433.
[36] A.S. Maria Chong, X.S. Zhao, A.T. Kustedjo, S.Z. Qiao, Functionalization of large-pore mesoporous silicas with organosilanes by direct synthesis, Microporous Mesoporous Mater. 72 (2004) 33-42.
[37] F. Hoffmann, M. Cornelius, J. Morell, M. Fröba, Silica-Based Mesoporous Organic–Inorganic Hybrid Materials, Angew. Chem. Int. Ed. 45 (2006) 3216-3251.
[38] T. Yokoi, H. Yoshitake, T. Tatsumi, Synthesis of amino-functionalized MCM-41 via direct co-condensation and post-synthesis grafting methods using mono-, di- and tri-amino-organoalkoxysilanes, J. Mater. Chem. 14 (2004) 951-957.
[39] A. Szegedi, M. Popova, I. Goshev, J. Mihály, Effect of amine functionalization of spherical MCM-41 and SBA-15 on controlled drug release, J. Solid State Chem. 184 (2011) 1201-1207.
[40] J. Ortiz-Bustos, A. Martín, V. Morales, R. Sanz, R.A. García-Muñoz, Surface-functionalization of mesoporous SBA-15 silica materials for controlled release of methylprednisolone sodium hemisuccinate: Influence of functionality type and strategies of incorporation, Microporous Mesoporous Mater. 240 (2017) 236-245.
[41] A. L. Doadrio, A. J. Salinas, J. M. Sánchez-Montero, M. Vallet-Regi, Drug release from ordered mesoporous silicas, Curr. Pharm. Des 21 (2015) 6213-6819.
[42] Y. Xu, C. Wang, G. Zhou, Y. Wu, J. Chen, Improving the controlled release of water-insoluble emodin from amino-functionalized mesoporous silica, Appl. Surf. Sci. 258 (2012) 6366-6372.
[43] A. Martín, R.A. García, D.S. Karaman, J.M. Rosenholm, Polyethyleneimine-functionalized large pore ordered silica materials for poorly water-soluble drug delivery, J. Mater. Sci 49 (2013) 1437-1447.
[44] A. Zakeri Siavashani, M. Haghbin Nazarpak, F. Fayyazbakhsh, T. Toliyat, S.J.P. McInnes, M. Solati-Hashjin, Effect of amino-functionalization on insulin delivery and cell viability for two types of silica mesoporous structures, J. Mater. Sci. 51 (2016) 10897-10909.
[45] D. Zhao, J. Feng, Q. Huo, N. Melosh, G.H. Fredrickson, B.F. Chmelka, G.D. Stucky, Triblock copolymer syntheses of mesoporous silica with periodic 50 to 300 angstrom pores, Science 279 (1998) 548-552.
[46] S.A. Kozlova, S.D. Kirik, Post-synthetic activation of silanol covering in the mesostructured silicate materials MCM-41 and SBA-15, Microporous Mesoporous Mater. 133 (2010) 124-133.
[47] J. M. Rosenholm, A. Penninkangas, M. Linden, Amino-functionalization of large-pore mesoscopically ordered silica bya one-step hyperbranching polymerization of a surface-grown polyethyleneimine, Chem. Comun. (2006) 3909-3911.
[48] R.A. Garcia-Munoz, V. Morales, M. Linares, P.E. Gonzalez, R. Sanz, D.P. Serrano, Influence of the structural and textural properties of ordered mesoporous materials and hierarchical zeolitic supports on the controlled release of methylprednisolone hemisuccinate, J. Mater. Chem. B 2 (2014) 7996-8004.
[49] M. Kruk, C.M. Hui, Synthesis and characterization of large-pore FDU-12 silica, Microporous Mesoporous Mater. 114 (2008) 64-73.
[50] F. Rouquerol, J. Rouquerol, K. Sing, Adsorption by Powders and Porous Solids, Academic Press, London, 1999.
[51] E.B. Celer, M. Kruk, Y. Zuzek, M. Jaroniec, Hydrothermal stability of SBA-15 and related ordered mesoporous silicas with plugged pores, J. Mater. Chem. 16 (2006) 2824-2833.
[52] D. Carmona, F. Balas, J. Santamaria, Pore ordering and surface properties of FDU-12 and SBA-15 mesoporous materials and their relation to drug loading and release in aqueous environments, Mater. Res. Bull. 59 (2014) 311-322.
[53] L. Cao, M. Kruk, Short synthesis of ordered silicas with very large mesopores, RSC Advances 4 (2014) 331-339.

[54] I. Langmuir, The Adsorption of Gases on Plane Surfaces of Glass, Mica and Platinum, J. Am. Chem. Soc. 40 (1918) 1361-1403.
[55] H. Freundlich, Of the adsorption of gases. Section II. Kinetics and energetics of gas adsorption. Introductory paper to section II, Trans. Faraday Soc. 28 (1932) 195-201.
[56] R. Sips, On the Structure of a Catalyst Surface, J. Chem. Phys 16 (1948) 490-495.
[57] O. Redlich, D.L. Peterson, A Useful Adsorption Isotherm, J. Phys. Chem. 63 (1959) 1024-1024.
[58] D.D. Duong, Adsorption Analysis: Equilibria and Kinetics, Imperial College Press, London, 1998.
[59] R.W. Korsmeyer, R. Gurny, E. Doelker, P. Buri, N.A. Peppas, Mechanisms of solute release from porous hydrophilic polymers, Int. J. Pharm. 15 (1983) 25-35.
[60] M.L. Bruschi, Mathematical models of drug release, Strategies to Modify the Drug Release from Pharmaceutical Systems, Woodhead Publishing 2015, pp. 63-86.
[61] K.M. Gallagher, O.I. Corrigan, Mechanistic aspects of the release of levamisole hydrochloride from biodegradable polymers, J. Control. Release 69 (2000) 261-272.
[62] M. Ishiyama, H. Tominaga, M. Shiga, K. Sasamoto, Y. Ohkura, K. Ueno, A Combined Assay of Cell Vability and in Vitro Cytotoxicity with a Highly Water-Soluble Tetrazolium Salt, Neutral Red and Crystal Violet, Biol. Pharm. Bull 19 (1996) 1518-1520.
[63] J. Zhang, D. Desai, J.M. Rosenholm, Tethered Lipid Bilayer Gates: Toward Extended Retention of Hydrophilic Cargo in Porous Nanocarriers, Adv. Funct. Mater. 24 (2014) 2352-2360.
[64] P. Schmidt-Winkel, W.W. Lukens, P. Yang, D.I. Margolese, J.S. Lettow, J.Y. Ying, G.D. Stucky, Microemulsion Templating of Siliceous Mesostructured Cellular Foams with Well-Defined Ultralarge Mesopores, Chem. Mater. 12 (2000) 686-696.
[65] Q. Huo, D.I. Margolese, G.D. Stucky, Surfactant Control of Phases in the Synthesis of Mesoporous Silica-Based Materials, Chem. Mater. 8 (1996) 1147-1160.
[66] W. Lin, Q. Cai, W. Pang, Y. Yue, B. Zou, New mineralization agents for the synthesis of MCM-41, Microporous Mesoporous Mater. 33 (1999) 187–196.
[67] S. Yang, L. Zhao, C. Yu, X. Zhou, J. Tang, P. Yuan, D. Chen, D. Zhao, On the Origin of Helical Mesostructures, J. Am. Chem. Soc. 128 (2006) 10460-10466.
[68] T. Yu, H. Zhang, X. Yan, Z. Chen, X. Zou, P. Oleynikov, D. Zhao, Pore structures of ordered large cage-type mesoporous silica FDU-12s, J. Phys. Chem. B 110 (2006) 21467-21472.
[69] F. Kleitz, L.A. Solovyov, G.M. Anilkumar, S.H. Choi, R. Ryoo, Transformation of highly ordered large pore silica mesophases (Fm3m, Im3m and p6mm) in a ternary triblock copolymer-butanol-water system, Chem. Commun. (2004) 1536-1537.

Supplementary Information

Synthesis procedure of pure silica materials

SBA-15 was synthesized according to the procedure described by Zhao et al. [45] applying triblock copolymer Pluronic P123 as a template and tetraethylorthosilicate (TEOS) as a source of silica. During the synthesis 4g of P-123 was dissolved in 125 mL of aqueous HCl 1.9 M at room temperature. After complete dissolution of co-polymer, 8 g of TEOS was added and the obtained mixture was stirred 20 h at 40 ℃. Next, the suspension was transferred into a tightly closed vessel and kept for 24 h at 110 ℃ without stirring. The obtained white solid was filtered and washed repeatedly with deionized water. The air-dry white powder was next calcinated at 550℃ for 5 h (heating rate 1.8℃·min^{-1}).

A one-day synthesis of LP-SBA-15 was as follows [53]. 2.4 g of Pluronic P123 surfactant ($EO_{20}PO_{70}EO_{20}$) and 0.027 g of NH_4F were dissolved using a mechanical stirrer in 84.0 mL of 1.30 M aqueous HCl solution at a selected initial temperature 17℃. After 30 minutes, a mixture of 5.5 mL TEOS and 1 g of 1,3,5- triisopropylbenzene (TIPB) was added and the resulting synthesis mixture was stirred for one hour at the same temperature in an open polypropylene container. Afterwards, the mixture was moved into a closed Teflon-lined autoclave and heated in an oven set at 130 ℃ during 3 hours. As-synthesized surfactant-templated silica was isolated as the usual procedure.

At the same way, a short synthesis of ULP-SBA-15 was carrying out with a similar procedure modifying the initial temperature to dissolve the surfactant (12.5℃) and the amount of TIPB (3.6 mL). A well as, the ageing temperature was 130℃ kept for 6h.

By increasing the silica over surfactant ratio in the synthesis of SBA-15, Plugged Hexagonal Templated Silica (PHTS) is formed [51]. For that, 4 g of P123 were dissolved in 130 mL of water and 20 mL HCl (37%) at room temperature. Then, 15 g of TEOS were added and the mix was

stirred at 60℃ during 7.5 h and aged at 80℃ for 15.5 h. The product was recovered with the same process that the rest of mesoporous silicas.

Mesostructured Cellular Foam (MCF) was prepared by a one-pot synthesis according to a procedure proposed by Stucky et al [64]. At first, 4 g of Pluronic 123 was dissolved in 150 g of 1.6 M HCl solution at 35-40℃. Then 4.6 mL of 1,3,5-trimethylbenzene and 0.047 g of NH_4F were added under vigorous stirring. Following 1 h of stirring, 9.14 mL of TEOS was added. The final mixture was stirred at 35-40℃ for 20 h and then transferred into a polypropylene bottle and heated at 100 ℃ under static conditions for 24 h. The solid product was recovered by filtration, washed with distilled water and dried at room temperature. The template was removed from the as-synthesized material by calcination at 550°C for 5 h under static conditions.

The SBA-3 synthesis procedure was taken from the literature [65]. Cetyltrimethylammonium bromide (CTAB) and tetraethyl orthosilicate (TEOS) were used as surfactant and silica source, respectively. An aqueous solution of HCl (37%) was used to adjust the pH value of the reaction system. 1.96 g of CTAB and 34.1 mL of HCl (37%) were dissolved in 79.3 mL of deionized water. TEOS (10 mL) was then added dropwise to the acidic CTAB solution while it was stirred at 500 rpm at room temperature. After 3 h, the resultant white precipitate (as-synthesized SBA-3) was filtered without washing and dried at 100℃ overnight. The as-synthesized SBA-3 powder was calcined at 550 ℃ in air for 5 h before characterization. The heating rate to 550℃ was 1.8℃ · min^{-1}.

A typical synthesis of MCM-41 sample, Lin et al. [66], is as follow: 2.52 g of cetyl trimethylammonium bromide (CTAB), 95.3 g distilled water and 7.83 g of dimethylamine (DMA) were combined at ambient temperature. After a homogeneous mixture has formed, 9.84 g of TEOS was added dropwise under stirring. After this, the mixture was stirred for a further 4 h and was then loaded into a tightly closed vessel following by heating at 110℃ for 48 h. The product was recovered by filtration, washing with distilled water and air dried. A detemplated sample

was obtained by calcination of the as-synthesized sample at 550℃ for 5 h (heating rate 1.8℃ · min^{-1}).

The synthesis of siliceous helical mesoporous material (MH) with hexagonal structure was based on the method described by Yang and co-workers [67], under basic conditions using cetyltrimethylammonium bromide (CTAB) and perfluorooctanoic acid (PFOA) as cotemplates. A typical synthesis was performed as follows: 0.20 g of CTAB was dissolved in 96 g of deionized water, stirring at room temperature for 30 min. Then, 0.7 mL of NaOH (2 M) and 0.02 g of PFOA were added separately into the solution. The temperature of the solution was raised and kept at 80℃ for 2 h. To this solution, 1.34 mL of tetraethyl orthosilicate (TEOS) was added. The mixture was continuously stirred for an additional 2 h. The resulting products were collected by filtration and dried at room temperature. The templates were removed by calcination at 550℃ for 5 h (1.8℃ · min^{-1}rate).

The formation of cubic pore-expanded LP-FDU-12 were similar to those reported by others [68], but modified to reduce the duration of the synthesis that was as follows. 1.0 g of Pluronic F127 ($EO_{106}PO_{70}EO_{106}$) copolymer and 5 g of KCl were dissolved using a mechanical stirrer in 61 mL of 2.0 M aqueous HCl solution at 15 ℃. After 30 minutes, 1.4 mL of TIPB was introduced. After 30 minutes of constant stirring, 4.5 mL of TEOS was added and the mixture was stirred for 3 hours in an open polypropylene container. Afterwards, the product was moved into a closed Teflon-lined autoclave and heated at 170℃ for 4.5 hours. As-synthesized silica was isolated by filtering without washing and calcined under air at 550℃ for 5 h (heating ramp 1.8℃ · min^{-1}).

3D cage-like mesoporous silica SBA-16 (*p6mm*) was synthesized using the copolymer Pluronic F127 template and butanol at low acid concentration according to the procedure described by Kleitz et al [69]. For this synthesis, 2.68 g of Pluronic F127 was dissolved in 128.6 g of distilled water and 5.8 g of HCl (37%) and stirred at room temperature until its completed dissolution. Thereafter, 8 g of 1-butanol was added and stirred for 1 h at 45℃. Then, 12.7 g of TEOS were dropwise added to the solution under vigorous stirring for 24 h at 45℃ to obtain the

mesostructured product. The resultant mixture was transferred to a Teflon-coated autoclave and aged for 24 h at 100°C. The solid white product was the filtered, washed with distilled water and dried. To remove the copolymer template, the solid is then calcined at 550°C for 5 h (heating ramp 2°C $\cdot$ min^{-1}).

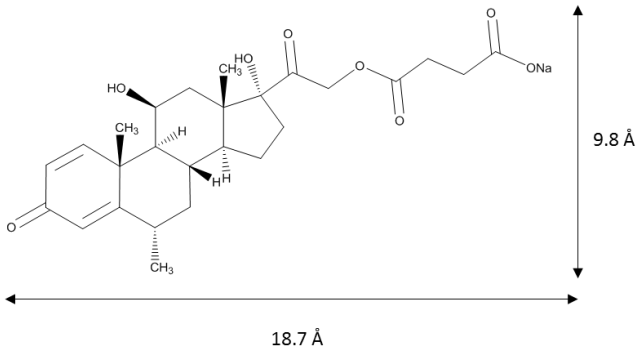

Scheme S1. Chemical structure of the methylprednisolone sodium succinate corticoid

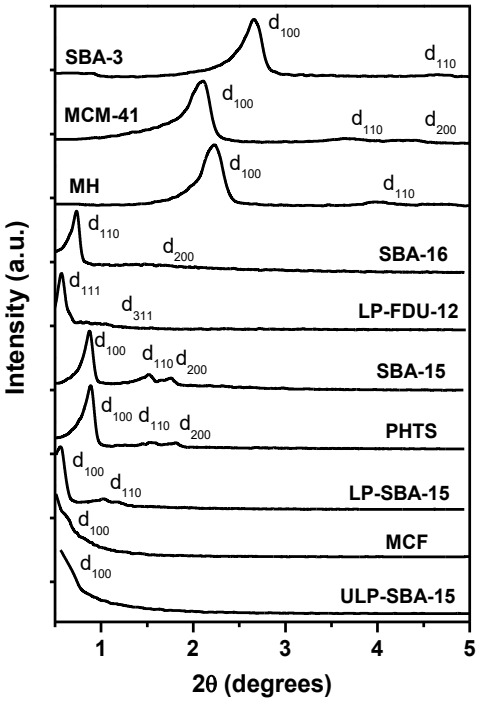

Figure S1. Low-angle XRD patterns recorded for pure silica materials

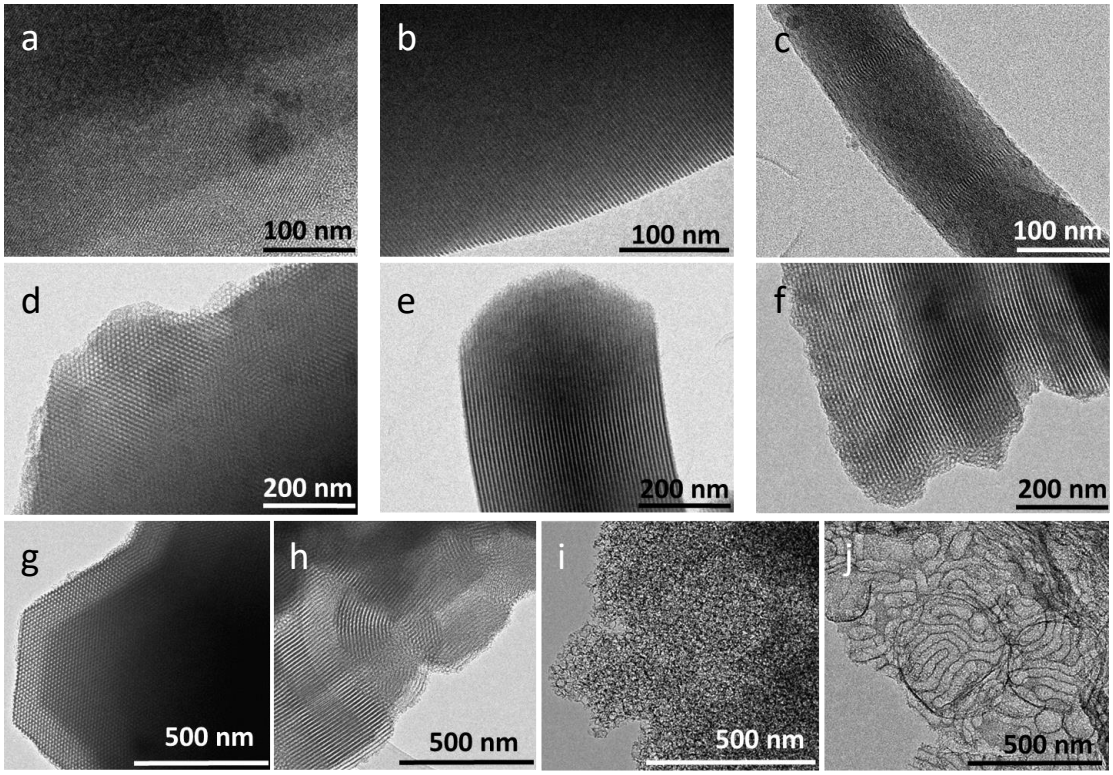

Figure S2. TEM micrographs of SBA-3 (a), MCM-41 (b), MH (c), SBA-16 (d), SBA-15 (e), PHTS (f), LP-FDU-12 (g), LP-SBA-15 (h), MCF (i) and ULP-SBA-15 (j).

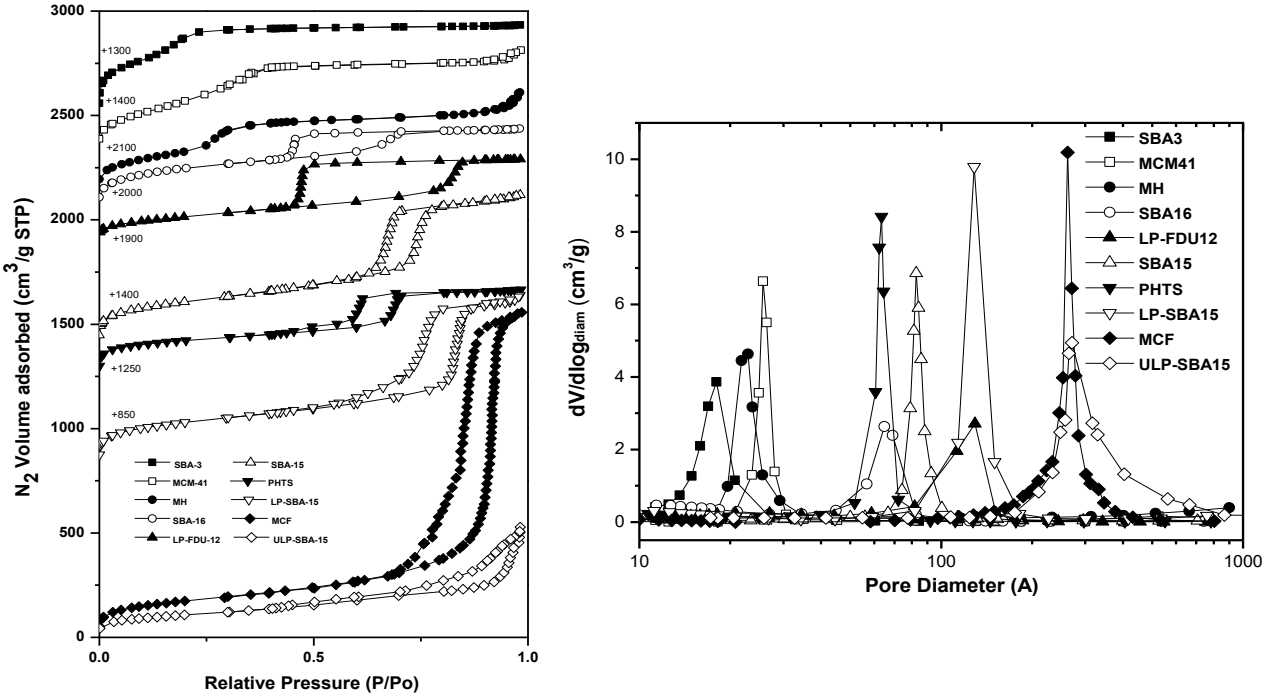

Figure S3. Nitrogen adsorption isotherms at 77 K for pure silica materials (left plot) and pore size distribution (right plot).

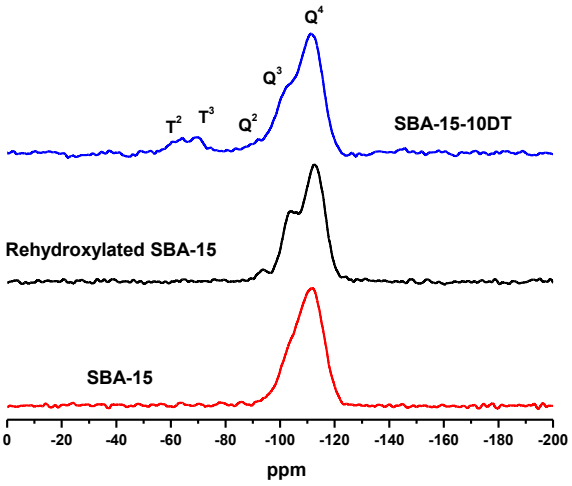

Figure S4. ^{29}Si MAS RMN spectra of the SBA-15 samples

Table S1. Fitting parameters for Langmuir, Freundlich, Sips and Redlich-Peterson models for the adsorption isotherms of methylprednisolone sodium succinate on silica materials at 298 K.

Material	Langmuir			Sips			
	Q_m (mg·g^{-1})	b (L·mg^{-1})	r^{2*}	Q_m (mg·g^{-1})	b (L·mg^{-1})	n	r^{2*}
SBA-3	235 ± 49	0.03 ± 0.01	0.980	148 ± 33	0.06 ± 0.02	1.4 ± 0.3	0.982
MCM-41	163 ± 15	0.06 ± 0.01	0.984	239 ± 134	0.03 ± 0.03	0.8 ± 0.2	0.984
MH	198 ± 11	0.12 ± 0.02	0.985	256 ± 74	0.06 ± 0.05	0.7 ± 0.2	0.986
SBA-16	160 ± 18	0.05 ± 0.01	0.981	179 ± 80	0.04 ± 0.04	0.9 ± 0.3	0.978
LP-FDU-12	177 ± 33	0.06 ± 0.02	0.948	114 ± 7	0.12 ± 0.01	2.3 ± 0.5	0.981
SBA-15	316 ± 45	0.04 ± 0.01	0.978	220 ± 36	0.08 ± 0.02	1.4 ± 0.3	0.981
PHTS	155 ± 13	0.11 ± 0.03	0.968	127 ± 10	0.16 ± 0.03	1.6 ± 0.4	0.976
LP-SBA-15	290 ± 24	0.09 ± 0.02	0.981	229 ± 18	0.13 ± 0.02	1.5 ± 0.2	0.988
MCF	186 ± 8	0.22 ± 0.04	0.983	165 ± 8	0.27 ± 0.03	1.5 ± 0.3	0.986
ULP-SBA-15	149 ± 7	0.21 ± 0.04	0.977	155 ± 23	0.20 ± 0.08	0.9 ± 0.3	0.974

Material	Freundlich			Redlich-Peterson			
	K_F (L^n·g^{-n})	n	r^{2*}	Q_m (mg·g^{-1})	b (L·mg^{-1})	n	r^{2*}
SBA-3	9 ± 2	0.72 ± 0.08	0.961	177 ± 12	0.025 ± 0.001	4.7 ± 1.4	0.993
MCM-41	17 ± 2	0.54 ± 0.05	0.976	85 ± 91	0.2 ± 0.3	0.7 ± 0.3	0.982
MH	37 ± 4	0.43 ± 0.04	0.971	167 ± 68	0.2 ± 0.1	0.9 ± 0.2	0.984
SBA-16	14 ± 3	0.57 ± 0.06	0.966	194 ± 15	0.032 ± 0.008	1.5 ± 0.6	0.979
LP-FDU-12	15 ± 6	0.59 ± 0.12	0.884	211 ± 9	0.031 ± 0.002	2.9 ± 0.8	0.981
SBA-15	19 ± 4	0.65 ± 0.07	0.954	312 ± 13	0.027 ± 0.001	3.2 ± 0.7	0.993
PHTS	27 ± 7	0.45 ± 0.08	0.893	234 ± 7	0.045 ± 0.005	1.9 ± 0.3	0.989
LP-SBA-15	38 ± 9	0.51 ± 0.08	0.925	403 ± 8	0.039 ± 0.003	1.9 ± 0.3	0.994
MCF	53 ± 9	0.34 ± 0.06	0.908	252 ± 29	0.12 ± 0.03	1.2 ± 0.1	0.987
ULP-SBA-15	43 ± 6	0.33 ± 0.05	0.923	200 ± 32	0.11 ± 0.04	1.2 ± 0.2	0.977

* For a proper comparison between different fittings regardless the number of experimental data points and model parameters, correlation coefficients (r^2) are adjusted to the degrees of freedom for each fitting.

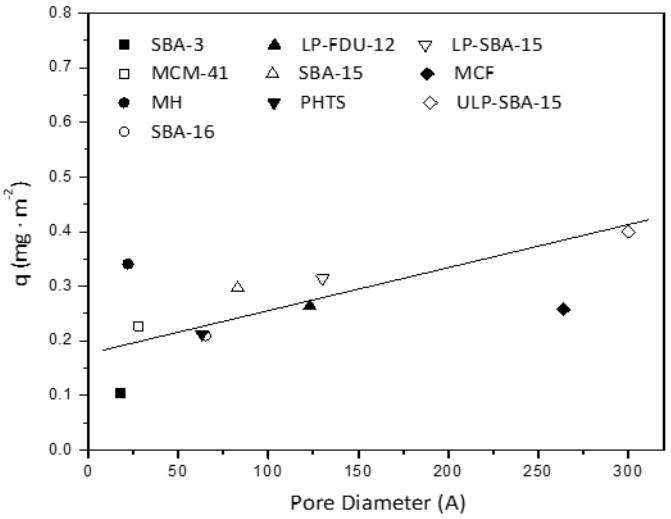

Figure S5. Experimental adsorption isotherms for the adsorption of drug per unit of specific BET surface area versus pore diameter on pure silica materials (b).

Table S2. Fitting parameters for Langmuir, Freundlich, Sips and Redlich-Peterson models for the adsorption isotherms of methylprednisolone sodium succinate on amino-modified silica materials at 298 K.

Material	Langmuir			Sips			
	Q_m (mg·g^{-1})	b (L·mg^{-1})	r^{2*}	Q_m (mg·g^{-1})	b (L·mg^{-1})	n	r^{2*}
SBA-3-10DT	370 ± 43	0.10 ± 0.03	0.958	273 ± 12	0.16 ± 0.01	2.1 ± 0.3	0.986
MCM-41-10DT	569 ± 53	0.16 ± 0.05	0.951	455 ± 12	0.21 ± 0.01	2.4 ± 0.3	0.992
MH-10DT	454 ± 30	0.18 ± 0.04	0.971	375 ± 9	0.25 ± 0.02	1.9 ± 0.2	0.995
SBA-16-10DT	562 ± 68	0.12 ± 0.04	0.943	422 ± 14	0.20 ± 0.01	2.5 ± 0.4	0.988
LP-FDU-12-10DT	658 ± 105	0.13 ± 0.06	0.896	491 ± 15	0.18 ± 0.01	3.3 ± 0.6	0.983
SBA-15-10DT	696 ± 103	0.11 ± 0.04	0.922	502 ± 20	0.18 ± 0.01	2.8 ± 0.5	0.979
PHTS-10DT	589 ± 61	0.17 ± 0.06	0.934	469 ± 8	0.22 ± 0.01	2.8 ± 0.3	0.994
LP-SBA-15-10DT	604 ± 51	0.22 ± 0.07	0.941	492 ± 5	0.30 ± 0.01	2.5 ± 0.1	0.998
MCF-10DT	610 ± 44	0.26 ± 0.08	0.953	514 ± 4	0.28 ± 0.01	2. 7 ± 0.1	0.999
ULP-SBA15-10DT	692 ± 123	0.10 ± 0.04	0.914	485 ± 26	0.17 ± 0.02	2.9 ± 0.7	0.968

Material	Freundlich			Redlich-Peterson			
	K_F (L^n·g^{-n})	n	r^{2*}	Q_m (mg·g^{-1})	b (L·mg^{-1})	n	r^{2*}
SBA-3-10DT	54 ± 17	0.5 ± 0.1	0.878	533 ± 15	0.043 ± 0.005	2.0 ± 0.4	0.986
MCM-41-10DT	152 ± 44	0.3 ± 0.1	0.719	901 ± 37	0.057 ± 0.008	1.8 ± 0.2	0.987
MH-10DT	106 ± 26	0.39 ± 0.08	0.864	714 ± 25	0.071 ± 0.007	1.6 ± 0.1	0.995
SBA-16-10DT	98 ± 32	0.5 ± 0.1	0.839	854 ± 30	0.050 ± 0.007	2.0 ± 0. 4	0.981
LP-FDU-12-10DT	144 ± 59	0.4 ± 0.1	0.625	1010 ± 47	0.048 ± 0.009	2.1 ± 0.6	0.949
SBA-15-10DT	113 ± 41	0.5 ± 0.1	0.775	1015 ± 41	0.047 ± 0.008	2.1 ± 0.5	0.964
PHTS-10DT	167 ± 53	0.3 ± 0.1	0.660	952 ± 48	0.060 ± 0.01	1.8 ± 0.3	0.977
LP-SBA-15-10DT	168 ± 47	0.4 ± 0.1	0.738	958 ± 77	0.09 ± 0.02	1.5 ± 0.2	0.976
MCF-10DT	226 ± 55	0.27 ± 0.09	0.659	990 ± 69	0.09 ± 0.02	1. 5 ± 0.2	0.984
ULP-SBA15-10DT	97 ± 38	0.5 ± 0.1	0.816	977 ± 41	0.043 ± 0.007	2.4 ± 0.7	0.956

* For a proper comparison between different fittings regardless the number of experimental data points and model parameters, correlation coefficients (r^2) are adjusted to the degrees of freedom for each fitting.

Table S3. Fitting parameters for Korsmeyer-Peppas, first-order and Gallagher-Corrigan kinetic models for the cumulative release of methylprednisolone sodium succinate on mesoporous silica materials at 335 K.

Material	Korsmeyer-Peppas			First-order		
	K_{KP} (mg·g^{-1}·d^{-n})	n	r^{2*}	K (d^{-1})	f_{max} (mg·g^{-1})	r^{2*}
SBA-3	121 ± 21	0.60 ± 0.05	0.9867	7.3 ± 0.3	56.8 ± 0.4	0.9899
MCM-41	124 ± 26	0.42 ± 0.05	0.9808	17 ± 1	62.8 ± 0.6	0.9741
MH	365 ± 47	0.82 ± 0.05	0.9926	5.8 ± 0.2	109 ± 1	0.9910
SBA-16	122 ± 17	0.57 ± 0.04	0.9902	7.9 ± 0.6	52 ± 1	0.9694
LP-FDU-12	100 ± 10	0.26 ± 0.03	0.9899	14 ± 2	77 ± 2	0.8237
SBA-15	212 ± 13	0.48 ± 0.02	0.9973	13.9 ± 0.7	101.0 ± 0.7	0.9851
PHTS	402 ± 47	0.75 ± 0.04	0.9959	10.8 ± 0.5	92 ± 1	0.9902
LP-SBA-15	404 ± 25	0.66 ± 0.02	0.9986	12.1 ± 0.6	111 ± 1	0.9838
MCF	543 ± 43	0.70 ± 0.03	0.9978	12.9 ± 0.6	131.4 ± 0.9	0.9915
ULP-SBA-15	396 ± 93	0.72 ± 0.07	0.9824	10.5 ± 0.5	97 ± 1	0.9868

Material	Gallagher-Corrigan					
	f_1 (mg·g^{-1})	k_1 (d^{-1})	f_2 (mg·g^{-1})	k_2 (d^{-1})	t_{max} (d)	r^{2*}
SBA-3	43 ± 1	12.5 ± 0.6	28 ± 2	5.0 ± 0.6	0.53 ± 0.06	0.9982
MCM-41	52 ± 1	21 ± 2	39 ± 3	2.3 ± 0.6	0.4 ± 0.1	0.9929
MH	94 ± 2	7.9 ± 0.3	77 ± 3	2.3 ± 0.5	1.3 ± 0.1	0.9985
SBA-16	35 ± 1	17 ± 14	18 ± 2	3.4 ± 0.3	0.62 ± 0.05	0.9970
LP-FDU-12	48 ± 4	39 ± 7	13 ± 7	1.7 ± 0.3	0.6 ± 0.2	0.9679
SBA-15	58 ± 5	27 ± 4	15 ± 10	14 ± 2	0.14 ± 0.01	0.9957
PHTS	80 ± 1	14.7 ± 0.3	68 ± 2	4.0 ± 0.6	0.69 ± 0.08	0.9993
LP-SBA-15	94 ± 3	16 ± 1	74 ± 5	2.9 ± 0.6	0.5 ± 0.1	0.9949
MCF	117 ± 1	16.3 ± 0.4	100 ± 3	3.8 ± 0.6	0.53 ± 0.08	0.9993
ULP-SBA-15	81 ± 2	15.8 ± 0.6	63 ± 4	4.7 ± 0.8	0.49 ± 0.08	0.9980

Table S4. Fitting parameters for Korsmeyer-Peppas, first-order and Gallagher-Corrigan kinetic models for the cumulative release of methyl prednisolone sodium succinate on mesoporous amino-modified silica materials at 335 K.

Material	Korsmeyer-Peppas			First-order		
	K_{KP} ($mg \cdot g^{-1} \cdot d^{-n}$)	n	r^{2*}	K (d^{-1})	f_{max} ($mg \cdot g^{-1}$)	r^{2*}
SBA-3-10DT	470 ± 19	0.69 ± 0.02	0.9984	5.3 ± 0.2	232 ± 1	0.9957
MCM-41-10DT	236 ± 8	0.47 ± 0.03	0.9809	1.03 ± 0.08	358 ± 6	0.9591
MH-10DT	127 ± 1	0.59 ± 0.01	0.9960	0.55 ± 0.03	291 ± 3	0.9899
SBA-16-10DT	293 ± 9	0.61 ± 0.02	0.9971	1.3 ± 0.1	331 ± 6	0.9679
LP-FDU-12-10DT	183 ± 2	0.69 ± 0.02	0.9975	0.57 ± 0.02	417 ± 4	0.9966
SBA-15-10DT	203 ± 2	0.60 ± 0.01	0.9974	0.73 ± 0.03	397 ± 5	0.9908
SBA-15-30DT	176 ± 3	0.53 ± 0.02	0.9934	0.56 ± 0.03	402 ± 6	0.9869
PHTS-10DT	495 ± 20	0.67 ± 0.03	0.9950	2.4 ± 0.1	420 ± 5	0.9886
LP-SBA-15-10DT	321 ± 6	0.68 ± 0.01	0.9990	1.25 ± 0.04	392 ± 3	0.9943
LP-SBA-15-30DT	329 ± 7	0.70 ± 0.01	0.9988	1.31 ± 0.03	394 ± 2	0.9968
MCF-10DT	507 ± 25	0.74 ± 0.03	0.9939	1.7 ± 0.1	473 ± 7	0.9862
MCF-30DT	316 ± 9	0.57 ± 0.02	0.9889	0.92 ± 0.05	543 ± 8	0.9862
ULP-SBA-15-10DT	193 ± 2	0.72 ± 0.02	0.9974	0.60 ± 0.01	425 ± 3	0.9979

Material	Gallagher-Corrigan					
	f_1 ($mg \cdot g^{-1}$)	k_1 (d^{-1})	f_2 ($mg \cdot g^{-1}$)	k_2 (d^{-1})	t_{max} (d)	r^{2*}
SBA-3-10DT	205 ± 4	6.0 ± 0.2	174 ± 9	1.9 ± 0.4	0.9 ± 0.1	0.9991
MCM-41-10DT	219 ± 7	2.9 ± 0.2	65 ± 14	0.88 ± 0.06	2.5 ± 0.1	0.9971
MH-10DT	248 ± 4	0.34 ± 0.01	193 ± 9	10 ± 1	0.18 ± 0.02	0.9991
SBA-16-10DT	212 ± 13	0.59 ± 0.05	76 ± 27	12 ± 1	0.14 ± 0.02	0.9956
LP-FDU-12-10DT	394 ± 4	0.50 ± 0.01	365 ± 8	19 ± 5	0.12 ± 0.02	0.9993
SBA-15-10DT	277 ± 20	1.1 ± 0.1	150 ± 39	0.8 ± 0.1	3.0 ± 0.3	0.9970
SBA-15-30DT	359 ± 3	0.42 ± 0.01	308 ± 6	32 ± 7	0.06 ± 0.01	0.9990
PHTS-10DT	340 ± 7	3.30 ± 0.09	245 ± 14	1.6 ± 0.1	1.7 ± 0.1	0.9993
LP-SBA-15-10DT	280 ± 7	2.07 ± 0.09	163 ± 15	1.48 ± 0.09	1.69 ± 0.08	0.9993
LP-SBA-15-30DT	281 ± 7	2.20 ± 0.07	166 ± 13	1.97 ± 0.09	1.51 ± 0.05	0.9997
MCF-10DT	378 ± 6	2.57 ± 0.05	260 ± 12	1.3 ± 0.1	2.5 ± 0.1	0.9995
MCF-30DT	293 ± 14	2.5 ± 0.2	42 ± 28	1.7 ± 0.1	1.89 ± 0.08	0.9989
ULP-SBA-15-10DT	407 ± 4	0.55 ± 0.01	384 ± 8	20 ± 7	0.11 ± 0.03	0.9993

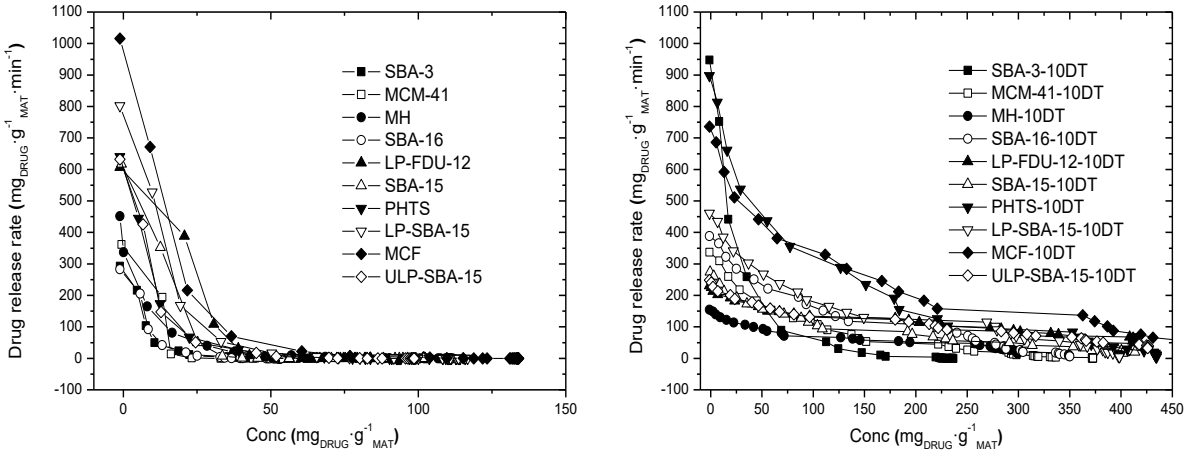

Figure S6. Instantaneous release rates of methylprednisolone species from pure and amino-functionalized mesoporous silica materials into simulated body fluid (PBS buffer) at pH=7.4 and 37 ℃. The instantaneous release rate values represent the derivative of a given cumulative release profile at a specific point in time.

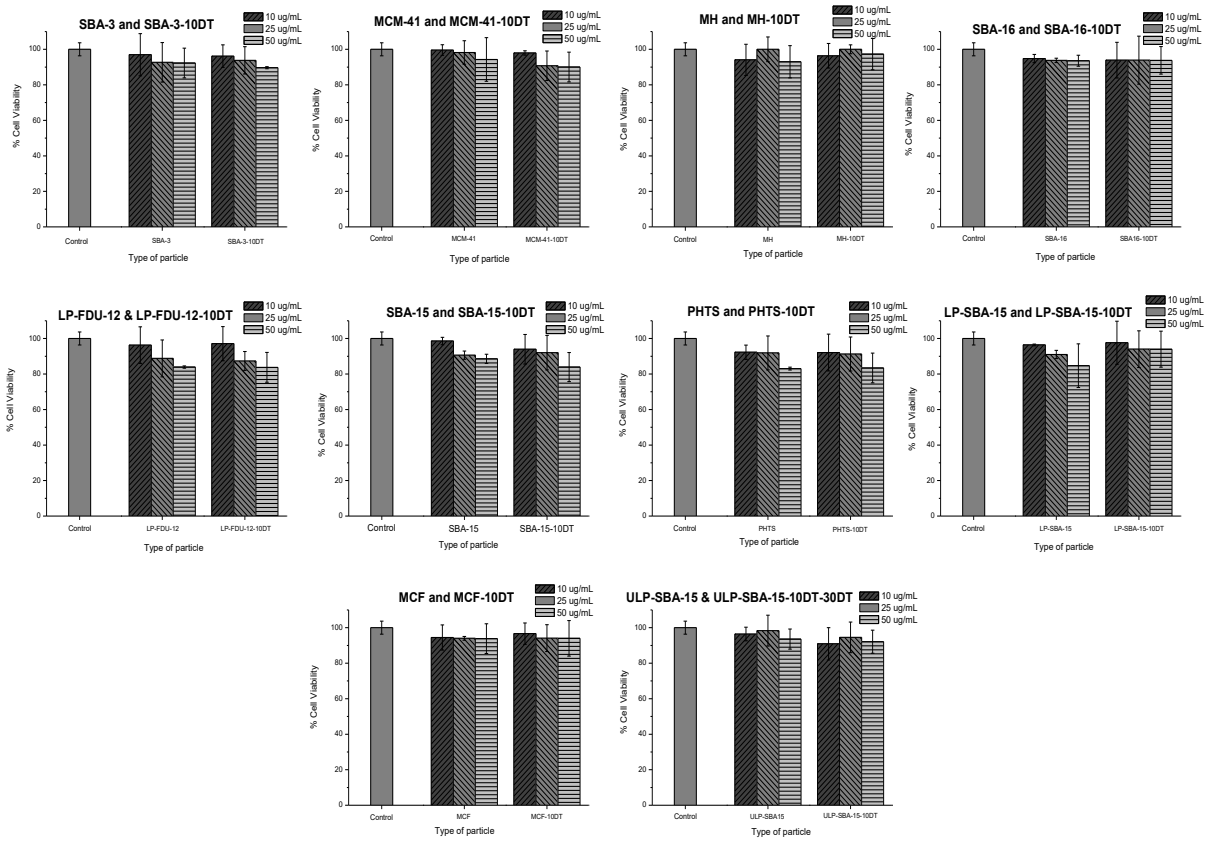

Figure S7. *In vitro* dose dependent cytocompatibility of pure and amino-functionalized materials after 72 h of incubation time on MDA-MB-231 Breast cancer cell lines. Cell viability was measured by the WST-1 assay. Error bars represent SD ($n \geq 3$)